

**Environmentally-Preferred
Advanced Generation**

Durability of Catalytic Combustion Systems

APPENDIX IV: Fuel/Air Premixer Development

Gray Davis, *Governor*



RESOURCES AGENCY

**November 2001
CALIFORNIA
ENERGY
COMMISSION**

CALIFORNIA ENERGY COMMISSION

Prepared for:

**CALIFORNIA ENERGY
COMMISSION**

Avtar Bining, Contract Manager
ENGINEERING OFFICE

Prepared by:

**Chris Weakley
John Payne
Tom Dowdy
Floyd Fleming**

Mike Batham, Program Lead
**Environmentally-Preferred
Advanced Generation**

**CATALYTICA ENERGY
SYSTEMS
Mountain View, CA**

Contract No. 500-97-033

Contract Amount: \$1,316,030

Legal Notice

This report was prepared as a result of work sponsored by the California Energy Commission (Commission, Energy Commission). It does not necessarily represent the views of the Commission, its employees, or the State of California. The Commission, the State of California, its employees, contractors, and subcontractors make no warranty, express or implied, and assume no legal liability for the information in this report; nor does any party represent that the use of this information will not infringe upon privately owned rights. This report has not been approved or disapproved by the Commission nor has the Commission passed upon the accuracy or adequacy of this information in this report.

Table of Contents

<u>Section</u>	<u>Page</u>
Preface	1
I. Executive Summary	2
II. Introduction	2
III. Program Approach	3
3.1 CFD Analysis of Flow path (Task 4.1)	3
3.2 Design and Fabrication of Cold Flow Rig Hardware (Task 4.2)	3
3.3 Cold Flow Testing (Task 4.3).....	3
3.4 Flow path Flame Holding Tests (Task 4.4).....	4
IV. Statement of Work	4
V. Background	5
5.1 Introduction	5
5.2 Lobed Forced Mixer – Background	6
5.3 Decision to Use Xonon® 1	8
VI. Design & Development of Axial Premixer - Lobed mixer CFD	9
6.1 Introduction	9
6.2 Geometry and Flow Conditions	9
6.3 Flow and model conditions	10
6.4 CFD Model Results	10
6.5 Comparison of Lobed Mixer Performance to Three-Stack Axial Mixer	13
6.6 Conclusions	15
6.7 Recommendations	15
VII. Fuel Peg CFD Analysis and Design	16
7.1 Background	16
7.2 Airfoil Design.....	17
7.3 CFD Model.....	18
7.4 Baseline Fuel Peg CFD	20
7.5 Airfoil CFD Models	21
7.6 Conclusions and Recommendations.....	22
VIII. Cold Flow Testing of Premixer	22
8.1 Introduction	22
8.2 Test Setup / Procedure.....	22
8.2.1 Hardware	22
8.2.2 Test Setup - Instrumentation	23
8.2.3 Summary – Test Run #1	24
8.2.4 Discussion and Conclusions.....	25
IV. Flameholding Study – UCI, Experimental Analysis	26

9.1	Background and Introduction.....	26
9.2	Literature Review.....	26
9.3	Experimental Apparatus.....	27
9.3.1	Test Conditions.....	27
9.3.2	Hardware.....	27
9.3.3	Data Acquisition.....	29
9.3.4	Prescreening Test Matrix.....	30
9.4	Results.....	31
9.4.1	Observations and Anomalies.....	31
9.4.2	Velocity Distribution.....	32
9.4.3	Turbulence Intensity.....	33
9.4.4	Fuel Distribution.....	34
9.4.5	Flameholding Results.....	34
9.5	Discussion.....	34
9.6	Summary, Conclusions, and Recommendations.....	36
9.6.1	Summary.....	36
9.6.2	Conclusions.....	36
9.6.3	Recommendations.....	37
X.	Flameholding Study – CSE, Simulation & Analysis.....	37
10.1	Introduction.....	37
10.2	Background.....	37
10.3	CFD Model.....	38
10.4	Perfectly-Stirred Reactor Model.....	39
10.5	Residence Time and Volume Determination.....	39
10.6	Lean Blowout Criteria.....	40
10.7	Results and Discussion.....	41
10.7.1	Flameholding Analysis.....	42
10.8	Summary and Conclusions.....	42
XI.	Conclusions and Future Work.....	43
	References.....	44
	Appendix A.....	A1
	Appendix B.....	B1
	Appendix C.....	C1
	Appendix D.....	D1
	Appendix E.....	E1
	Appendix F.....	F1

List of Figures

<u>Figure</u>	<u>Page</u>
Figure 4.1 -- Work flow diagram for axial premixer analysis effort.....	4
Figure 5.2.1 -- Schematic of a Typical Ejector.....	6
Figure 5.2.2 -- Lobed Mixer.....	6
Figure 5.2.3 -- Vortex development, flow over a Lobed Mixer.....	6
Figure 5.2.4 -- Example of Lobed Mixer in Turbofan application.....	7
Figure 5.3.1 -- CESI Xonon®1 combustor.....	8
Figure 6.2.1 -- Three-dimensional rendering of a complete lobed mixer along with fuel pegs....	10
Figure 7.1.1 -- Baseline Fuel-Peg Geometry and Two-Layer Computational Grid.....	17
Figure A1 -- Schematic of a Typical Ejector.....	A1
Figure A2 -- Schematic of a Lobed Mixer.....	A1
Figure A3 -- Vortex development, flow over a Lobed Mixer.....	A1
Figure A4 -- Example of Lobed Mixer in Turbofan application.....	A1
Figure A5 -- CESI Xonon® combustor, KHI engine.....	A2
Figure B1 – Turbojet Engine with Lobe Mixer.....	B1
Figure B2 – Lobe Mixer Geometry.....	B1
Figure B3 – Mixing Effects Produced by Lobe Mixer.....	B2
Figure B4 – Three-dimensional Rendering of Lobe Mixer.....	B2
Figure B5 – Lobe Mixer Geometry Features.....	B3
Figure B6 – Features of Lobe Mixer Geometry Cross-section at Lobe Exit.....	B3
Figure B7 – Edge Scalar Injection Points.....	B4
Figure B8 – Scalar Injection Locations Cross-section.....	B4
Figure B9 – In-Plane Velocity Vectors with Short-Lobe Mixer.....	B5
Figure B10 – Velocity Vector Plots with Long 12-Lobe Geometry.....	B5
Figure B11 – Ten Lobe Mixer In-Plane Velocities.....	B6
Figure B12 – Twelve Lobe Mixer In-Plane Velocities.....	B6
Figure B13 – Fifteen Lobe In-Plane Velocity.....	B7
Figure B14 – Ten Lobe Scalar Axial Concentrations.....	B7
Figure B15 – Twelve Lobe Scalar Axial Concentrations.....	B8
Figure B16 – Fifteen Lobe Scalar Axial Concentrations.....	B8
Figure B17 – Fifteen Lobe Scalar Axial Concentrations with Scalar 4 Moved.....	B9
Figure B18 – Three Dimensional Solid Model of 12 Lobe Mixer.....	B9
Figure B19 – Fuel Injection at the Outside of the Inward Directed Lobe.....	B10
Figure B20 – Fuel Injection at the Inside of the Outward Directed Lobe.....	B10
Figure B21 – Scalar Injection Directly Upstream of a Lobe.....	B11
Figure B22 – Scalar Flow Around an Inward Directed Lobe.....	B11
Figure B23 – Eight Scalar Injection Summary.....	B12
Figure B24 – Scalar Injection from Upstream Outward Directed Lobe Exit.....	B12
Figure B25 – Scalar Injection Half-way between Outward Directed Lobes.....	B13
Figure B26 – Scalar Concentrations for 15 Lobe Mixer with 8 Edge Injection Locations.....	B13
Figure B27 – 15 Lobe Mixer, 8 Edge Scalar Concentration for Range 0.5 to 1.5.....	B14
Figure B28 – Cross-stream Velocities Downstream of Lobe Mixer.....	B14
Figure B29 – Cross-Stream Velocities for 3-Stack Mixer.....	B15
Figure B30 – Turbulence Intensity – 15 Lobe Mixer.....	B15
Figure B31 – Turbulence Intensity – 3-Stack Mixer.....	B16

Figure B32 – Turbulent to Laminar Viscosity Ratio – 15 Lobe Mixer.....	B16
Figure B33 – Turbulent to Laminar Viscosity Ratio – 3-Stack Mixer.....	B17
Figure C1 – Baseline Fuel-Peg Geometry and Two-Layer Computational Grid.....	C1
Figure C2 – NACA0033 Fuel-Peg Geometry and Two-Layer Computational Grid.....	C1
Figure C3 – Typical y^+ Values on Fuel-Peg Surface for CFD Simulations.....	C2
Figure C4 – Typical Near-Wall Cells (Red) in Two-Layer CFD Model.....	C2
Figure C5 – Fuel-Peg U-Velocity Magnitude at 12.5° Approach Angle.....	C3
Figure C6 – Fuel-Peg U-Velocity Magnitude at 13° Approach Angle (1000 Iterations – Not Converged).....	C3
Figure C7 – NACA0027 Fuel-Peg U-Velocity Magnitude at 14° Approach Angle.....	C4
Figure C9 -- NACA0030 Fuel-Peg U-Velocity Magnitude at 14° Approach Angle.....	C5
Figure C10 – NACA0030 Fuel-Peg U-Velocity Magnitude at 18° Approach Angle.....	C5
Figure C11 – NACA0033 Fuel-Peg U-Magnitude at 12° Approach Angle.....	C6
Figure C12 – NACA0033 Fuel-Peg U-Magnitude at 16° Approach Angle.....	C6
Figure C13 – NACA0036 Fuel-Peg U-Magnitude at 10° Approach Angle.....	C7
Figure C14 – NACA0036 Fuel-Peg U-Magnitude at 14° Approach Angle.....	C7
Figure D1-- Lobe Mixer and Fuelpegs (2 views).....	D1
Figure D2 -- CS view of Lobe Mixer installed in cold flow rig.....	D1
Figure D3 -- Schematic of Lobe Mixer cold flow rig instrumentation.....	D2
Figure D4 -- Location of wedge probe instrumentation.....	D3
Figure D5 -- Fuel / air sampling grid points.....	D3
Figure D6 -- Measured HC Conc. vs. Angle and Diameter.....	D4
Figure D7 -- HC Meas. Deviation vs Radial Distance.....	D4
Figure D8 -- HC Meas. Deviation versus Angle.....	D5
Figure D9 -- Outer Sample Deviations versus Angle.....	D5
Figure E1 -- Overall Schematic of the Experimental Apparatus.....	E5
Figure E2 -- Photograph of the Overall Setup.....	E5
Figure E3 -- Photograph of the Mixing/Conditioning Section.....	E5
Figure E4 -- Test Section Schematic.....	E6
Figure E5 -- Photograph of Test Section.....	E6
Figure E6 -- Test Section Overview.....	E7
Figure E7 -- Water Quench Schematic.....	E7
Figure E8 -- Photograph of Laser Anemometry.....	E8
Figure E9 -- Predicted Weak Extinction Limit for Matrix Shown in Table E3.....	E8
Figure E10 -- Hydrogen Igniter.....	E9
Figure E11 -- Flameholding at the Step.....	E9
Figure E12 -- Flameholding Upstream.....	E9
Figure E13 -- Contours of Mean Axial Velocity, m/s.....	E10
Figure E14 -- % Deviation from Mean of Axial Velocities.....	E11
Figure E15 -- Mean Axial Velocity Results Plotted as Surface Maps for Four Conditions.....	E12
Figure E16 -- Contours of Local Turbulence Intensity, u'/U	E13
Figure E17 -- Turbulence Intensity and Velocity Contours for High Turbulence Case.....	E14
Figure E18 -- Measured Fuel Distribution.....	E14
Figure E19 -- % Deviation from Mean for Natural Gas Concentrations.....	E15
Figure E20 -- Comparison of Current Results with Choudhury and Cambel.....	E16

Figure E21 -- Comparison of Current Weak Extinction Limits at the Prediction of Ballal and Lefebvre classified by Step Expansion Height.....	E17
Figure E22 -- Correlation Using Local Equivalence Ratio Values for Measured WE values.....	E17
Figure E23 -- Results from ANOVA-Model A.....	E18
Figure E24 -- Results from ANOVA-Model B.....	E19
Figure E25 -- Summary Plot of Measured Weak Extinction Limits.....	E20
Figure F1 -- Step Flameholder 3D CFD model.....	F1
Figure F2 -- Recirc. Zone velocity, 10% from wall, 1" and 2".....	F1
Figure F3 -- Recirc. Zone velocity, 20% from wall, 1" and 2".....	F2
Figure F4 -- Recirc. Zone velocity, 30% from wall, 1" and 2".....	F2
Figure F5 -- Recirc. Zone velocity, 40% from wall, 1" and 2".....	F3
Figure F6 -- Recirc. Zone velocity, 50% from wall, 1" and 2".....	F3
Figure F7 -- Wall shear, 2".....	F4
Figure F8 -- Wall shear, 1".....	F4
Figure F9a -- In-plane velocity grid, 0.2" downstream of step.....	F5
Figure F9b -- In-plane velocity gradient, 0.2" downstream of step.....	F5
Figure F10a -- In-plane velocity grid, 0.4" downstream of step.....	F6
Figure F10b -- In-plane velocity gradient, 0.4" downstream of step.....	F6
Figure F11a -- In-plane velocity grid, 0.6" downstream of step.....	F7
Figure F11b -- In-plane velocity gradient, 0.6" downstream of step.....	F7
Figure F12a -- In-plane velocity grid, 0.8" downstream of step.....	F8
Figure F12b -- In-plane velocity gradient, 0.8" downstream of step.....	F8
Figure F13a -- In-plane velocity grid, 1.0" downstream of step.....	F9
Figure F13b -- In-plane velocity gradient, 1.0" downstream of step.....	F9
Figure F14 -- Backward facing step.....	F10
Figure F15 -- Velocity gradient, 10% from wall, full section.....	F11
Figure F16 -- Velocity gradient, 20% from wall, full section.....	F11
Figure F17 -- Velocity gradient, 30% from wall, full section.....	F12
Figure F18 -- Velocity gradient, 40% from wall, full section.....	F12
Figure F19 -- Velocity gradient, 50% from wall, full section.....	F13

List of Tables

<u>Table</u>	<u>Page</u>
Table 6.4.1 -- Location of individual scalar locations.....	12
Table 7.3.1 -- Fuel-Peg Model Conditions and Methods.....	19
Table 7.4.1 -- Approach Angles and Velocity Components.....	20
Table 7.5.1 -- Airfoil Fuel Peg CFD Simulations Approach Angle and Figure Numbers.....	21
Table 8.2.1.1 -- Location and size of holes to be drilled in fuelpegs.....	23
Table 8.2.2.1 -- Fuel/Air Sample Point Locations.....	24
Table 10.3.1 -- Inlet Conditions.....	39
Table 10.7.1 -- Reattachment Length using the standard k- ϵ model with Chen modification.....	41
Table 10.7.1.1 -- Recirculation Zone Volume and Time.....	42
Table E1 -- Operating Conditions and Parameter List.....	E1
Table E2 -- Geometric Conditions and Parameter List.....	E1
Table E3 -- Planned Full Factorial Test Matrix for Sudden Expansion Wall Perturbation.....	E2
Table E4 -- Final Test Matrix Conducted.....	E3
Table E5 -- Results of Test Matrix for Sudden Expansion Wall.....	E4

Preface

The Public Interest Energy Research (PIER) Program supports public interest energy research and development that will help improve the quality of life in California by bringing environmentally safe, affordable, and reliable energy services and products to the marketplace.

The PIER Program, managed by the California Energy Commission (Commission), annually awards up to \$62 million to conduct the most promising public interest energy research by partnering with Research, Development, and Demonstration (RD&D) organizations, including individuals, businesses, utilities, and public or private research institutions.

PIER funding efforts are focused on the following six RD&D program areas:

- Buildings End-Use Energy Efficiency
- Industrial/Agricultural/Water End-Use Energy Efficiency
- Renewable Energy
- Environmentally-Preferred Advanced Generation
- Energy-Related Environmental Research
- Strategic Energy Research

What follows is a topical report for the **Durability of Catalytic Combustion Systems Project**, conducted by Catalytica Energy Systems Inc. The report is entitled “**Fuel-Air Premixer Development.**” This project contributes to the Environmentally-Preferred Advanced Generation program.

For more information on the PIER Program, please visit the Commission's Web site at: <http://www.energy.ca.gov/research/index.html> or contact the Commission's Publications Unit at 916-654-5200.

I. Executive Summary

As a part of the CEC funded program “Durability of Catalytic Combustion Systems”, CESI conducted a study to design, develop, and test a mixer / fuel injection system for an axial flow combustor. In order for CESI’s catalytic combustor to have acceptable performance, an axial flow mixer must provide a fuel / air mixture with uniform composition, velocity and temperature to the catalyst with mixing occurring over a very short distance and with a low pressure drop.

The mixer that was developed was a lobed forced mixer that can achieve good mixing over a relatively short distance. The fuel pegs chosen for this mixer were an airfoil design which reduces dynamic pressure losses and flow recirculation, thus decreasing the potential for flameholding. The primary benefit of this design is reduced package size for an axial flow combustor without decreasing catalyst life. The design focused on the CESI Xonon® 1 catalytic combustion system for the Kawasaki M1A-13X gas turbine, since this was the most readily available and easily utilized engine test bed at the time.

The following steps were completed for this study:

- A background literature search to determine the best mixer configuration to pursue for this study.
- CFD analyses of various lobed mixer and fuel peg parameters in order to determine the optimum geometry for the final design.
- Experimental and analytical analyses to better understand flameholding mechanisms for this mixer design and future design iterations.
- Cold flow rig testing of the final mixer / fuel peg designs to determine the fuel-air mixing characteristics of the mixer.

Fuel-air concentration profiles from cold flow testing of the initial designs indicated that additional development of the mixer was needed before on-engine testing could be conducted. The original proposal specified that engine hot-testing of the new mixer would follow the cold flow tests, but the marginal mixing improvements from the early designs did not justify devoting program resources to the hot testing tasks and the associated new hardware. Additional design work will be required in order that the CESI axial premixer technology can be fully exploited.

II. Introduction

The following document contains a summary of the CESI Axial Premixer design and development work that was conducted as a part of the California Energy Commission-funded program for the proposal titled “Durability of Catalytic Combustion Systems”. The proposal description of the procedure and deliverables for completion of Axial Premixer development (Task 4 in the proposal) is given below.

In conducting the premixer development task, all the effort was directed at Tasks 4.1 – 4.4. Tasks 4.5 – 4.7 involving, respectively, the design, fabrication, and testing of an on-engine mixer were not undertaken; and CEC funds allocated for those tasks were not used. Further work will be

required in order that the CESI axial premixer technology can be fully developed. Detailed descriptions of CESI activities for each Task addressed make up the remainder of this document.

III. Program Approach

The fuel-air premixer for a catalytic combustor is designed to provide a homogeneous mixture to the face of the catalyst. This is essential for the long life operation of the catalyst and has been achieved by CESI engineers through design iterations, rig and engine testing. The pre-mixer includes the fuel injection pegs upstream of the mixer and the flow path between the mixer and the catalyst face. The current premixer designs are for use with a “reverse flow” burner system. Other designs are now being considered for “inline” preburners which do not have the 180 degree-turn at the premixer location.

3.1 CFD Analysis of Flow path (Task 4.1)

Computational Fluid Dynamics (CFD) is being used extensively to evaluate mixer and flow-path designs. In addition to mixing the fuel and air, the mixer and flow path must be designed without recirculation. The areas of recirculation are potential flameholders and need to be avoided so that high temperatures upstream of the catalyst do not occur. CESI designs based on CFD are now available which virtually eliminate recirculation areas, but engine hardware has not yet been built. This task is intended to take the rules developed for radial mixers used in reverse flow combustors and apply them to inline premixers. Since there are no inline combustor engine programs in progress at CESI, this premixer design will be incorporated in the current Kawasaki combustor. The results of the CFD analysis will be used to design cold flow test rig hardware to empirically verify the CFD results prior to building engine hardware.

3.2 Design and Fabrication of Cold Flow Rig Hardware (Task 4.2)

To support the CFD design for the inline premixer, a companion cold flow rig test program will be required. Task 4.2 will provide the design of the hardware based on the physical requirements of the inline premixer design and use the technology developed by CESI in the previous radial premixer test programs. The design will be such that it can be retrofitted into the Kawasaki engine at some point during the Task 1 testing. Task 1 testing with the inline mixer will still use the original catalyst and will proceed until the 8000 hours limit is reached with the catalyst.

3.3 Cold Flow Testing (Task 4.3)

Validation of the designs will be accomplished through testing in cold flow test rigs. A full size model will be used with a non-flammable fuel air mixture so that pressure and velocity measurements can be taken at strategic locations identified by the CFD analysis. Fuel uniformity will also be measured during the tests to evaluate the mixing effectiveness. A variety of fuel injection peg designs will be tested to optimize the fuel/air uniformity at the catalyst face. The cold flow rig will be instrumented so as to provide for velocity measurements to verify that recirculation zones do not exist. Instrumentation will also be provided to measure the fuel/air ratio at the face of the catalyst to verify good mixing. Tufts of yarn will also be installed inside the flow path so that visual observations can be made of the direction of airflow along the walls of the premixer.

3.4 Flow Path Flame Holding Tests (Task 4.4)

It is essential that the flow path upstream of the catalyst be free of regions that can hold flame. These are normally recirculation regions, or regions of very low velocity. CFD design with cold flow rig testing should give confidence that these regions do not exist. This task is designed to provide test validation that ignition will not occur in the flow path. Scale model test hardware will be designed and fabricated to simulate the engine flow path with igniters at strategic locations. With the appropriate fuel air mixture flowing at simulated design conditions, attempts will be made to ignite the mixture. Ignition will not be expected, but if it occurs, measurements will be taken to determine if the flame extinguishes before it could reach the catalyst.

IV. Statement of Work

The logical workflow for the development of the Axial Premixer can be summarized in the following diagram:

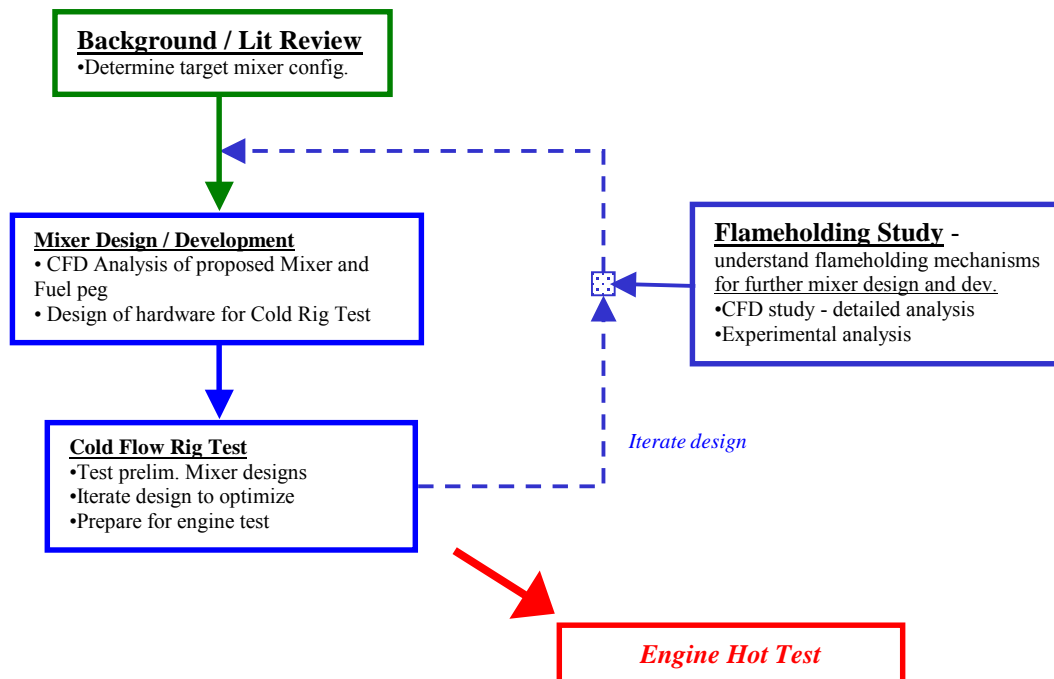


Figure 4.1 -- Work flow diagram for axial premixer analysis effort

The steps followed in this process can be further summarized as follows:

- A background data search / literature review was first conducted in order to isolate the mixer configuration. A review of previous studies led to the selection of a lobe forced mixer, as a short mixing length is required for an Axial Premixer. The airfoil design for the fuel peg was selected based on the requirements for low flow recirculation and minimum pressure loss.

- Once the hardware selection was completed, mixer and fuel peg designs were developed through detailed CFD analysis. Mixer test hardware was procured when the final design was obtained from the analyses.
- In parallel, experimental and analytical analyses were performed in order to better understand flameholding mechanisms. This information was useful for this mixer design and future design iterations.
- Cold flow rig testing was conducted with this design; however, initial results indicated that further work was needed in order to satisfy the mixing specification.
- Further design and development activity was conducted; however, the results ultimately did not warrant the expenditure for the engine hot test envisioned in the original program plan.

V. Background

5.1 Introduction

This Section discusses in detail the decision to pursue a lobed forced mixer for the Axial Premixer design as well as the choice to focus the premixer design, development, and testing activities on the Kawasaki M1A-13X engine configuration.

In a catalytic axial combustor system, a well-mixed stream is needed at the catalyst inlet with the following criteria:

- Low pressure drop across the fuel injection-mixer section in order to minimize pumping losses.
- Little or no flow recirculation in order to prevent flameholding where possible.
- The shortest possible mixing length in order to meet package spatial and weight constraints in addition to minimizing flow losses.

As will be discussed below, previous studies have shown that a lobed forced mixer can be used to achieve good mixing over a short distance. The use of an airfoil design for the fuel injection peg can reduce dynamic pressure losses and flow recirculation.

In order to minimize development time for the Premixer, CESI chose to simulate, cold rig test, and hot engine test the new Premixer system with a single, consistent combustor configuration. At the time the Premixer development program was being conducted, CESI had accumulated significant catalytic combustor development and testing experience with the Xonon®1 system on a Kawasaki 1.5 MW gas turbine. In addition, this was the only combustor-engine test bed that was readily available at the time. The cold rig test axial mixer configuration was to be designed so that, following completion of rig testing, it could be readily transferred to the Xonon®1 test engine.

5.2 Lobed Forced Mixer – Background

In many applications, it is important to effectively mix two co-flowing gaseous streams. One method, which has been used for many years, is an ejector or eductor. An ejector is a device which causes a high velocity fluid stream of given mass flow rate to converge into a fluid stream of lower velocity but greater mass flow rate. This convergence is achieved through the transfer of energy produced by the viscous interaction of the high velocity (primary) fluid stream with the lower velocity (secondary) fluid stream within a passage.

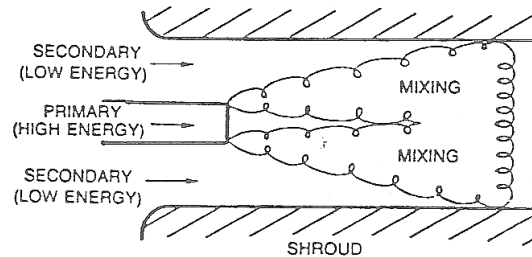


Fig 5.2.1 -- Schematic of a Typical Ejector

Shown in Figure 5.2.1 is a sketch of a simple ejector, here with the ejector passage being a solid walled duct. An exhausting high-energy primary flow entrains surrounding secondary fluid and increases its flow velocity, with the two streams then continuing to exchange energy via mixing as they proceed down the duct. The ejector's efficiency is defined as the ratio of the entrained secondary flowrate to that of the supplied primary flowrate. Effectiveness of the mixing process between the primary and secondary streams has been identified by numerous investigators as the key factor in determining the level of ejector efficiency. This effectiveness is related to the completeness of and the losses involved in the mixing process, both of which typically favor a mixing duct of long length. (Skebe 1988)

For most practical applications, however, the mixing duct length is limited by installation and weight requirements. Therefore, in order to improve ejector efficiency, research efforts have concentrated on developing ejectors that optimize the conflicting objectives of achieving a high rate of mixing with low primary flow losses within a short overall length.

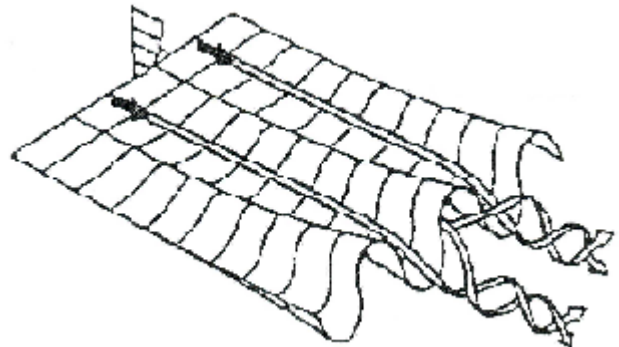


Figure 5.2.2-Lobed Mixer

One way to increase mixing between co-flowing streams is the introduction of strong, large-scale, streamwise vortices. The lobed mixer shown in Figure 5.2.2 embodies flow physics typical of a wide variety of mixing augmentation schemes designed to introduce axial vorticity. A variation in aerodynamic loading along the span of the mixer results in streamwise vorticity being shed into the downstream flow, analogous to the situation downstream of a finite wing. The streamwise vorticity which leaves the mixer trailing edge subsequently rolls up into discrete streamwise vortices, so that some distance downstream of the mixer

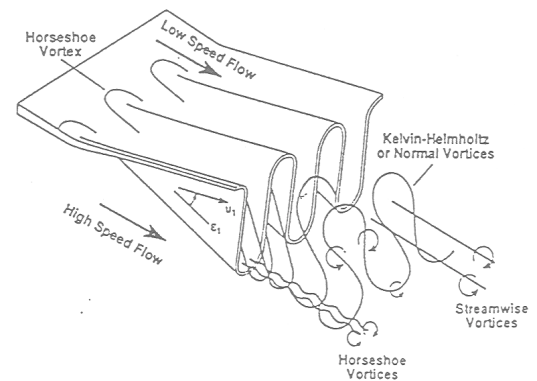


Figure 5.2.3 -- Vortex development, flow over a Lobed Mixer

there is an embedded array of streamwise vortices of alternating sign. (Waitz 1993)

A schematic showing the location of various vortical elements about a forced mixer is shown in Figure 5.2.3. The most prominent structures in the flow field are the counter-rotating pairs of streamwise vortices, shed as described above, and the Kelvin-Helmholtz or “normal vortices” associated with the velocity difference on either side of the plate. The scale of the streamwise structures is set by the wavelength of the lobes, whereas the initial scale of the normal vortices is set by the boundary layer height at the trailing edge, similar to a planar shear layer. In most applications, therefore, the scale of the normal vortices is a small fraction of the lobe height for at least several wavelengths downstream. Horseshoe vortices are formed around the front of the lobes but these are typically an order of magnitude weaker than either the normal or streamwise vortices and do not contribute strongly to the mixing process.

The augmentation in mixing provided by a lobed mixer above and beyond that in a planar shear layer can be attributed to two effects; both are associated with increasing the interfacial surface area between the flows on either side of the lobe. The first is the increase in contact area between the fluids due simply to the increased length of the convoluted trailing edge. The second is a further increase in contact area, which is generated as the interface is convected and stretched through the action of the streamwise vortices. Concomitant with this increase in interfacial surface area is a narrowing of gradient dimensions leading to a heightened mixing. Experiments and computations have been performed to separate the influence of increased trailing edge length from the influence of the shed streamwise vortices.

Conventional ejectors, which rely solely on viscous shear layer mixing, typically require long duct lengths in order to achieve good mixing results. This added duct length could result in substantial viscous losses. Using a combination of a lobed mixer on the jet exhaust nozzle, and an ejector shroud, a “mixer ejector” can be created which enhances the conventional mixing process by using large-scaled axial vorticity.

Work by Presz et al, (e.g. Presz 1991), has indicated that a substantial increase in the pumping performance of an ejector system can be obtained through the use of low loss ‘forced’ mixer lobes. These ‘forced’ mixers have proven very effective in advanced turbofan applications (Figure 5.2.4) by achieving nearly complete mixing of separate engine and fan streams with very low loss and within duct length-to-height ratios of unity. This behavior has been documented by Patterson (Barbu 1988). Effective mixing is accomplished through the generation of large-scale axial vorticity. This is achieved by merging the two streams after they have been given moderate absolute but strong relative secondary flow components as a result of their passage over opposite sides of a gently transitioned planar-to-three dimensional surface. (Skebe 1988)

Lobed mixers have seen significant development and application, primarily in the aircraft engine industry. The main reason for this development has been for thrust augmentation by entraining low temperature,

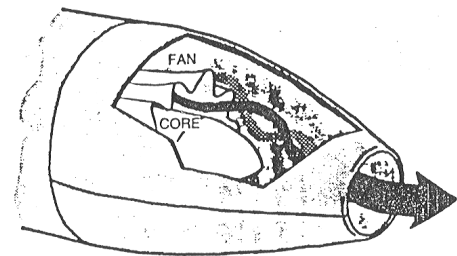


Figure 5.2.4 -- Example of Lobed Mixer in Turbofan application

low velocity, cooling air to increase the thrust, as shown in Fig. 5.2.4. The thrust is defined as the product of the mass flow of the jet times the jet velocity. An ideal augmentor is described as a device which maximizes thrust with a given energy transfer, while satisfying thermodynamic constraints. As engine temperature and velocities have increased, the exit velocity has also increased. The noise level from the engine is related to the peak velocity of the discharging stream to the seventh power (Presz 1991.) The environmental noise has been an additional driving force to develop lobed mixers.

CESI's interest in lobed mixers is generally to provide an axial flow mixer that will provide a uniform fuel/air mixture to the catalyst. This flow needs to have uniform composition, velocity and temperature. The mixing of fuel and air and the production of uniform temperature and velocities must occur in a very short mixing length and with a low pressure drop.

The goal of CESI is to obtain a uniform mixture, i.e., to obtain good mixing. The purpose of aerospace usage is thrust augmentation and noise reduction. However, these objectives are accomplished by obtaining good mixing in a short mixing length. Therefore, the lobed mixer is a viable option for an axial flow mixer.

The initial design of a lobed mixer will be for retrofit into a Xonon® combustor on the Kawasaki M1A-13X gas turbine. However, it may also prove to be an option for other applications that require an axial mixer.

5.3 Decision to Use Xonon® 1

The “Xonon® 1” combustor configuration is shown in cross-section in Figure 5.3.1. (CESI has developed newer catalytic combustor designs, designated Xonon® 2.0, 2.1, etc., for the M1A-13X turbine subsequent to this mixer development work.) It is equipped with three layers of radial swirlers located in the 180° reverse flow region. These swirlers would be removed, and the lobed mixer would be added in the straight, constant area between the turn and the catalyst. There is a center body extending from the dome through the catalyst, however, this should not present an inherent difficulty since it is also present in the turbofan engine design.

The Xonon® 1 has been tested, and CFD models have been performed with the current swirlers. Based upon the cross-sectional view of the Xonon® 1, it would be expected that flow separation would occur from the inside of the 180° turn, with a resulting higher mass and velocity occurring towards the centerline of the

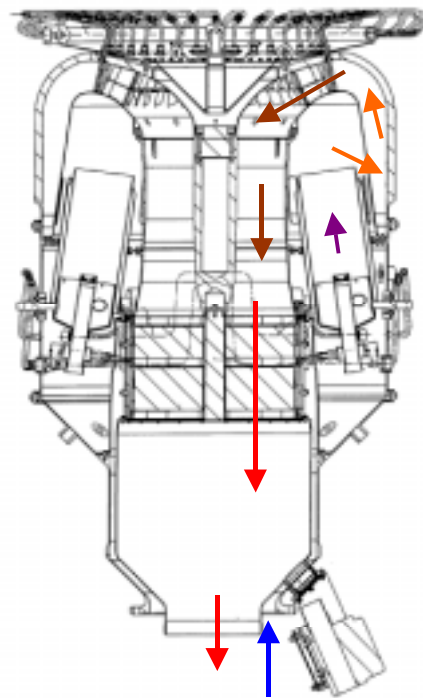


Figure 5.3.1 -- CESI Xonon® 1 combustor

catalyst. However, the area available for flow decreases markedly in the dome and axial approach to the catalyst. This should force more even flow.

VI. Design & Development of Axial Premixer - Lobed mixer CFD

6.1 Introduction

A computational simulation was conducted to study the feasibility, and establish design guidelines for using, a lobed mixer in a catalytic combustor. The lobed mixer would be used to assist mixing of the main fuel with the preheated preburner exit air. Simulations were conducted with varying lobe lengths, and number of lobes. The lobe shapes were generated through the rotation of a sine curve 360°. The centerline of the lobed mixer was located half way between the combustor center-body and the combustor wall. The Xonon® 1 flow path was used, with inlet flows mapped from separate preburner solutions conducted without the radial mixers.

The computational meshes were generated by hand and consisted of approximately 600,000 computational cells. High accuracy physical property and turbulent viscosity models were used based upon experience with earlier radial mixer simulations. Model results showed that the initial design based upon literature results did not provide sufficient penetration from the lobe exits to the walls of the combustor. The lobe length was increased for subsequent simulations, and adequate penetration was obtained.

Mixers with 10, 12 and 15 lobes were simulated. The mixing effectiveness increased as the number of lobes was increased. Most of this improvement is believed to be due to the implied increase in the number of fuel injection points, i.e., eight or sixteen for each lobe required for symmetry.

Comparison of results with the CFD results for the atmospheric pressure 3-Stack radial mixer model indicates that the current designed lobed mixer will not provide the degree of fuel/air uniformity provided by the radial mixer. The lobed mixer does not have the mixing driving mechanisms of strong swirl and counter-flow provided by the current radial mixer. The lobed mixer shows promise, however, as an alternate mixer, especially for axial flow combustors where a radial mixer might be difficult to design and install.

6.2 Geometry and Flow Conditions

The first run was made with a lobed mixer with a design based upon a good compromise between the several design parameters and guidelines found in the literature search. This resulted in geometry of:

Geometry of lobes analyzed

Lobe Shape	Sine curve
Number of Lobes, N_L	12 initially, later runs with 10 and 15
Diameter of Lobe Center	Half-way between center-body and preburner diameters
Lobe Amplitude, $(h/2)$	One-quarter distance between lobe center and preburner wall, initially. (Extended after first run to provide greater penetration.)

Lobe half-angle 22.5°

As an aid to visualization, Figure 6.2.1 shows a three-dimensional rendering of a complete lobed mixer along with fuel pegs. Note that all Figures discussed in this Section 6 of this report can be found in Appendix B. Due to the symmetry of the design, only a half-lobe was used in the

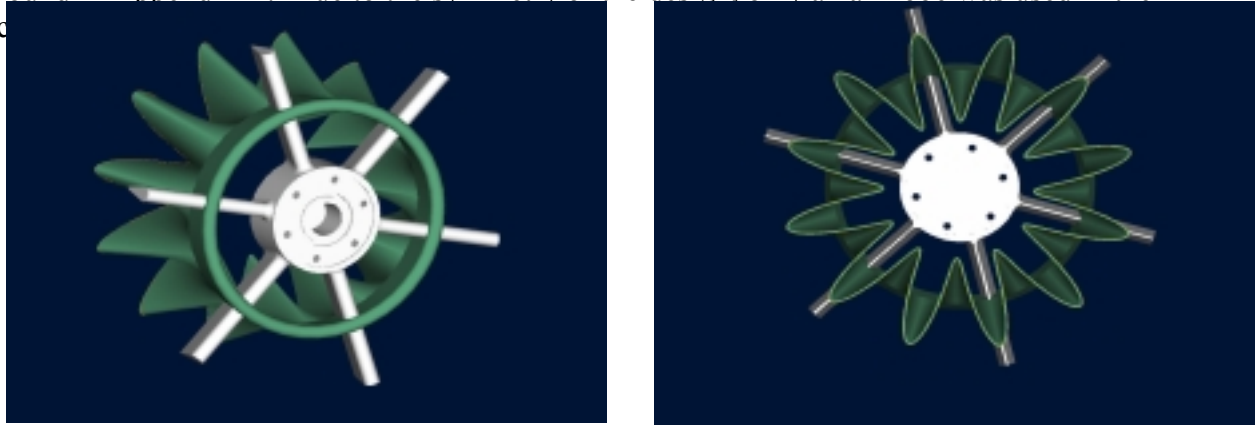


Figure 6.2.1 -- Three-dimensional rendering of a complete lobed mixer along with fuel pegs

6.3 Flow and model conditions

The lobe model was provided by CESI and sent to Combustion Science and Engineering (CSE) for CFD model mesh generation and simulation. A computational mesh of approximately 600,000 cells was used in this and other simulations. Figures B5 and B6 in Appendix B show features of the long 12-lobe geometry. The first simulation was made with an assumption that a high Reynolds number turbulence model was appropriate. A second simulation was made with a low Reynolds number turbulence model, which required a refined grid. These two simulations produced the same results, thus indicating that the high Reynolds number turbulence model was suitable.

The inlet boundary condition was taken from a previous run of the KHI premixer geometry with the radial mixers removed. This provided an inlet boundary condition that was then mapped to the inlet boundary of all simulation runs. The inlet boundary was essentially isothermal, but did have variation in the inlet axial and radial velocity components, and in the turbulence parameters κ (kappa – turbulent kinetic energy) and ϵ (epsilon – rate of turbulence dissipation).

6.4 CFD Model Results

The first simulation performed was on a 12-lobe mixer. The mixer centerline was located halfway between the centerbody and the combustor wall. The lobes expanded at a 22.5° half-angle outward for a distance such that the lobe exit was halfway between the mixer centerline and the outer (inner) walls of the combustor.

A key result of this simulation is shown in Figure B9. The main observation to be made is seen in the top drawing on this figure. This shows that the fluid flowing outward through the upward directed lobe is not reaching and mixing with the flow approaching axially from the upstream (left). The outward flowing air through the lobe is not penetrating to the wall, or in the nomenclature of mixers, this is an under-utilized case. Ideally, the momentum of the fluid flowing outward through the lobe would cause it to approach the surface very closely.

The second simulation made was with a 12-lobe mixer with the same location and half-angle, but with the lobes being extended downstream and outwards from the lobe centerline. The lobes were extended to within about one-half inch from the combustor wall and center-body. A plot similar to the previous plot can be found in Figure B10. In this case, as well in other cases run with longer lobes, the lobe jet penetration to the wall was very good. Since the penetration concern was adequately addressed with this first modification, all future runs were made with this longer lobe.

After obtaining a solution for the 12-lobe mixer that met the jet penetration requirement, computer models were also generated for 10-lobe and 15-lobe designs. The next important factor that was investigated was the mixing between the fluid inside and outside of each lobe. There are several ways to examine the mixing between the two streams. One way is to compare the in-plane velocities normal to the bulk axial flow direction. The in-plane velocities are shown in Figures B11, B12 and B13 for 10, 12 and 15 lobe models respectively. Little difference can be seen between these plots. In general, the degree of mixing (i.e., the cross-planar velocities) is low compared to the radial mixer currently in use in Xonon® 2.

A second way to compare the amount of mixing achieved between the different alternatives investigated is to inject tracers, called scalars, into each configuration. Axial and radial plots for each tracer location indicate how well the gas is mixing.

In all of the base cases, a default pattern of 8 symmetrically spaced scalar “injection” points was used. These give a relative indication of the mixing achieved with the change in number of lobes from 10 to 12 to 15. A single scalar can be made quantitative by normalizing the value and plotting the ratio of the local concentration of the scalar to the average concentration of that scalar. Thus, the individual scalar plots can be viewed as quantitative. The specific scalar locations are numbered by their locations. The following Table identifies these locations.

Scalar Number	Location Relative to Lobe Centerline	Quadrant
1	Outside	Upper Right
2	Outside	Lower Right
3	Outside	Lower Left
4	Outside	Upper Left
5	Inside	Upper Right
6	Inside	Lower Right
7	Inside	Lower Left
8	Inside	Upper Left

Table 6.4.1 -- Location of individual scalar locations

However, due to the method of “injecting” scalars, the combined plots of multiple scalars are only qualitative in nature. All scalars used have the same physical properties of the air flowing through the system. The technique that is used is to “mark” the air which passes through the 8 predefined volumes in the grid. Since the volumes of each grid region are different, and the velocity, density, etc., of the fluid flowing through each volume are different, the quantity of each scalar produced is different. Thus, the overall pattern of fluid from all scalars gives a qualitative view of scalar mixing and coverage, but cannot be considered to be quantitative.

Comparison of the scalars from the 10, 12 and 15 lobe models (Figures B14 – B16) shows that, at least qualitatively, the uniformity of mixing at the catalyst inlet improves with the number of lobes, with the 15-lobe mixer being the best. Note that this is at least partially due to the effective increased number of injection points around the 360° of the burner as the number of lobes is increased. For example, 8 injection points per half-lobe or 16 injection points per lobe would give 160 injection points for a 10 lobe swirler, 192 injection points for a 12 lobe swirler and 240 injection points for a 15 lobe swirler. Since the 15 lobe model gave the best overall coverage with the 8 symmetrically spaced injection points per half-lobe, this geometry was used in other runs to examine the effect of other injection point locations and number of injection points. (Note that a 12-lobe mixer was selected for cold flow tests due to mechanical requirements to more easily mate with existing equipment.)

Examination of the exit scalar concentration patterns indicates that a low concentration point is located at the upper left corner of the axial views. As a first small step towards improving the mixing pattern uniformity, the closest scalar, scalar 4, was moved radially outward and rotated counterclockwise toward the edge of the segment being modeled, i.e., placed directly upstream of the low concentration point. The solution of the scalar portion of the CFD problem was restarted (from zero scalar concentration) and converged to give the results shown in Figure B17. As seen, moving an injection point to a location directly upstream of this low concentration point was not effective in reducing the low concentration. (As will be shown below, moving the upper right-hand scalar, number 1, was actually more effective in filling this low concentration area.)

The scalar injections were initially located at eight points within the half-lobe being modeled, or 16 fuel injection points per full lobe. To reduce the number of injection points, the eight points were moved to the edges of the half-lobe. Due to symmetry, this is equivalent to having only eight fuel injection points per full lobe. This would tentatively allow the use of one fuel peg per lobe, with each fuel peg having 8 fuel injection jets. As an aid for visualization, Figure B18 shows a solid model of a 12-lobe mixer with 6 fuel pegs. (The final cold flow model design has 12 fuel pegs, each with 10 injection holes, for a 12-lobe mixer.)

The scalar solutions from the CFD runs show the following:

- A fuel feed point must be located at the inside of the outward directed lobes and at the outside of the inward directed lobes. This can be seen in Figures B19 and B20. In Figure B19 a fuel injection (maximum concentration) point is isolated at the outside (of the lobe centerline) of the inward directed lobe. The maximum concentration from this injection point can be traced from the injection point (Lobe Inlet) to the Lobe Outlet, then downstream

half-way to the catalyst and finally at the catalyst inlet. In the cold flow experiments, a perforated plate is used to simulate the pressure drop across the catalyst. Note that a single injection point is made quantitative by dividing the local concentration by the average concentration. The average concentration per unit time can only be calculated based upon the converged exit fluid flow, since the scalars are “created” in the interior of the flow field.

- Fuel injection directly upstream of a lobe produces fuel flow around the side of the lobes as shown in Figures B21 and B22. Both figures show that the high concentrations, especially at the lobe exit, occur at the sides of the lobes. The gas does not follow the lobe contour outward as might at first be expected.
- Figure B23 shows all eight scalars used for this specific run. Note that plots of all scalars used are semi-quantitative, since the total fuel exiting the flowfield is used as a divisor to normalize the concentrations. If the fuel injection rate at each of the scalar locations were the same, which is not true, a “perfectly mixed fluid” would have a uniform concentration of 1.0 at the exit. In Figure B23 note the low concentration level at the top center-left, halfway to the perforated plate. This low concentration point shows on all figures. This low concentration area is due to distance between injection points being farther apart at the outer diameter than at inner diameters. This indicates that a greater amount of fuel should be injected into this area. This is consistent with the fact that the area outside the lobe centerline is almost twice the area inside the lobe centerline.

Figures B24 and B25 show that obtaining full coverage at the outside of the lobed mixer and between the outward directed lobes is difficult. Figure B25 shows that a fuel injection point centered between the outward directed lobes helps increase fuel concentration in this area. However, Figure B24 indicates that fuel injection directly upstream of an outward directed lobe exit is even more effective in “moving” fuel toward the mid-point of the outward directed lobes.

Figure B26 shows results of modeling the 15-lobe mixer with eight scalar injection points moved outward to the edges of the half-lobe being modeled. The concentration is expressed on a normalized basis of the local concentration of the scalar divided by the average concentration over the flow domain. On a scale of 0.0 to 5.0 as used in Figure B26, the concentration looks relatively uniform. However, Figure B27 shows that on a scale of 0.5 to 1.5, the scalar concentration is not very uniform compared to that required to have a uniform fuel-to-air mixture. This is further discussed later in comparison to the three-stack mixer design.

6.5 Comparison of Lobed Mixer Performance to Three-Stack Axial Mixer

The objective of this study was to provide a preliminary performance assessment of the proposed lobed mixer geometry and to select a configuration (number of lobes, shape, length, etc) for a more detailed study. The criteria used to evaluate the lobed mixer performance are listed below:

1. Strength of secondary and cross flows
2. Turbulence levels
 - Turbulence Intensity
 - Turbulent Viscosity from Non-linear κ - ϵ turbulence model
3. Scalar concentrations from point source injections
4. Robustness

- Sensitivity to fuel injector fouling (plugging of fuel injector hole)
5. Low flame holding potential
 - Absence of recirculation / low velocity zones with ignitable fuel concentrations

These criteria were selected based on the flow characteristics observed in the Catalytica 3-stack mixer that has demonstrated superior mixing performance analytically, in the lab and in the field. The 3-stack mixer has a maximum cross flow velocity (swirl) of approximately 30 m/sec at atmospheric conditions. This high cross flow velocity, coupled with the +/- counter rotation induced by the 3-stack design, produces significant convective stirring, high turbulence levels, listed below, and a wide circumferential dispersal of fuel from the injection location. In addition, these flow characteristics were achieved in the 3-stack mixer without producing any high potential flame holding regions.

• Cross Flow Velocity	30 m/sec	
• Turbulence Levels	TI	65%
	Tub/Lam Vis	6,000

Lobe Performance

1. In developing the models for these geometries, it became clear that, due to symmetry, the lobed mixers will produce isolated circumferential “flow cells” covering $\frac{1}{2}$ of a lobe period or pitch. For example, in a 10-lobe design, 20 circumferential “flow cells” are produced. The lobes produce secondary flows that will convectively stir the flow within a cell, but fuel can move between cells only through diffusion (laminar & turbulent). Because of the isolated nature of these flow cells, there will be limited circumferential migration of the fuel aft of the lobes. The inability of the fuel to move circumferentially between flow cells limits the robustness of the mixer to injector fouling or plugging. Plugging will reduce fuel concentrations within the affected cell. Stated in another way, the lobed mixer does not impart any swirl to the gas mixture as does the axial mixer configuration. Therefore, there is no convective driving force to mix between adjacent lobes.
2. While the lobe geometries did produce organized secondary and cross-stream flows downstream of the lobes, these flows were not very strong. In all the lobe configurations studied, a peak cross-flow velocity of between 6 to 7 m/sec was produced aft of the lobes (Figure B28), which is significantly lower than that produced in the 3-stack mixer (Figure B29). The strength of the cross-flow velocity was influenced more by the length of the lobe geometry rather than by the number of lobes.
3. The turbulence levels in the lobed mixer are also significantly lower than observed in the 3-stack mixer, which is not surprising given the much weaker secondary flow and shear rates produced by the lobed mixer. Turbulence intensity levels in the diffuser were approximately 15% to 20% in the lobed mixer (Figure B30) versus 65% in the 3-stack design (Figure B31). Also, turbulence viscosity levels are 6 times lower in the lobed mixer (Figure B32) than in the 3-stack mixer (Figure B33). There are differences in turbulence levels for the various lobe configurations studied, but these differences are small compared to the gap between lobe designs and the 3-stack mixer.
4. Based on the scalar mixing results performed as part of these studies, it appears that more lobes produce a more mixed result. This result is at least partially due to the fact that the number of injection points increases in these analyses as the number of lobes increases.

5. Tracking of the fuel from individual fuel injection locations shows that the fuel from individual fuel injection locations does not fully mix within a lobe flow cell. In addition, the analyses identified injection locations that mix more readily than others did. Based on these results, it is likely that a fuel injection pattern can be developed that would produce a reasonably uniform fuel profile within an individual flow cell. However, it is not clear, without further more detailed CFD analyses, how the fuel profile would be affected by normal injector stack up and sizing variations.
6. A small recirculation zone did occur beneath the cylinder that forms the “leading edge” of the lobe geometry. This recirculation zone was caused by the non-uniform flow distribution occurring in the 180-degree bend upstream of the lobe, and is upstream of the fuel injection pegs. This zone could be eliminated by a number of techniques, such as employing upstream turning vanes or by tailoring the current (cylindrical) leading edge shape of the lobe to align it more with the incoming flow direction.

6.6 Conclusions

- The strength of the secondary flows and turbulence levels observed in the analyses of these lobed mixer configurations suggests that they will not perform at the same level as the 3-stack mixer design.
- Based on the results to date, it appears that more lobes produce a slightly better mixed result. However, this result may be due to the larger number of implied fuel injection location with an increasing number of lobes.
- The scalar mixing results suggest that a fuel injection pattern can be developed that would produce a reasonably well-mixed flow entering the catalyst. However, the results also suggest that the robustness of this design may be limited given the isolated nature of the flow cells produced by the lobes and the relatively weak secondary flow and low turbulence levels.

6.7 Recommendations

The lobed mixer shows promise for development as an alternate to the radial mixers currently being used. The initial sine curve form of the lobed mixer simulated results in a sharp peak at the inner and outer lobe exits. This results in a large (unmixed) area between the lobe exits, particularly on the outer edge. This unmixed area could be reduced by increasing the exit areas of the lobes. Instead of a sine curve, a shape with the lobe sides oriented along radial “spokes”, such as shown in Figures B2 and B3, would decrease the distance between lobe exit points by almost a factor of two.

A difference between the lobed mixer modeled and the traditional lobed mixer use can be noted by comparison to Figures B1 and B3. In the aeropropulsion applications, the inner gas flow is at a higher velocity and higher temperature than the outer gas flow. This type of geometry could be produced in a catalytic combustion preburner by designing the preburner to be the “inner” zone of an axial mixer. The preburner exit gas would be hotter, and can be designed to be faster than the outside compressor discharge “dilution” air. The main fuel would be injected into the dilution air upstream of the lobes, in locations similar to that used in the current simulations.

Since the simulations indicate that the design is probably not optimal, further CFD analysis is recommended. These simulations should be simplified, screening models, testing a wider range of geometries. Multiple geometries could now be produced relatively rapidly using an automatic meshing tool, such as SAMM. During this program, test meshes were generated by SAMM, but were not found to be acceptable for simulation. The basic problem is that the lobed mixer has a “natural” cylindrical coordinate system. When the hand generated meshes are studied, the mesh dimensions are “small” in the circumferential dimension, “medium” in the radial direction, and “large” in the axial direction. The version of SAMM used did not support cylindrical coordinates, so the lobed mixer geometry was “carved” from a cubic (or rectangular) solid, thus producing unacceptable results. The current version of SAMM fully supports cylindrical coordinates. It is recommended that additional simulations be performed with simplified geometry and modeling parameters to decrease computer run times and allow more cases (estimated about 12) to be run. One or more “final” designs can then be further refined and/or hand meshed for a more accurate simulation if required.

VII. Fuel Peg CFD Analysis and Design

7.1 Background

For good fuel and air mixing, it is important to obtain a good fuel distribution from the fuel injection system. This can be interpreted to mean obtaining a uniform fuel distribution and/or to inject the fuel in such a manner as to take maximum advantage of the mixing capability of the lobed mixer. Obtaining uniform fuel and air mixing only from the fuel injection system would be difficult, since a very large number of fuel injection points would be required.

The method for fuel injection successfully used by CESI is to use a fuel injector or fuel peg shaped as shown in Figure 7.1.1. Note that all figures discussed in Section 7 can be found in Appendix C. The cross-section is that of a circular tube with a triangular shaped faring welded onto the downstream side. Fuel injection holes are drilled perpendicular to the dominant air flow direction and the fuel peg. This provides small, high velocity jets of fuel, normally natural gas, to penetrate and mix with the air. The depth of fuel penetration is calculated by a method developed by CESI. The mixer then is used to increase the fuel and air uniformity.

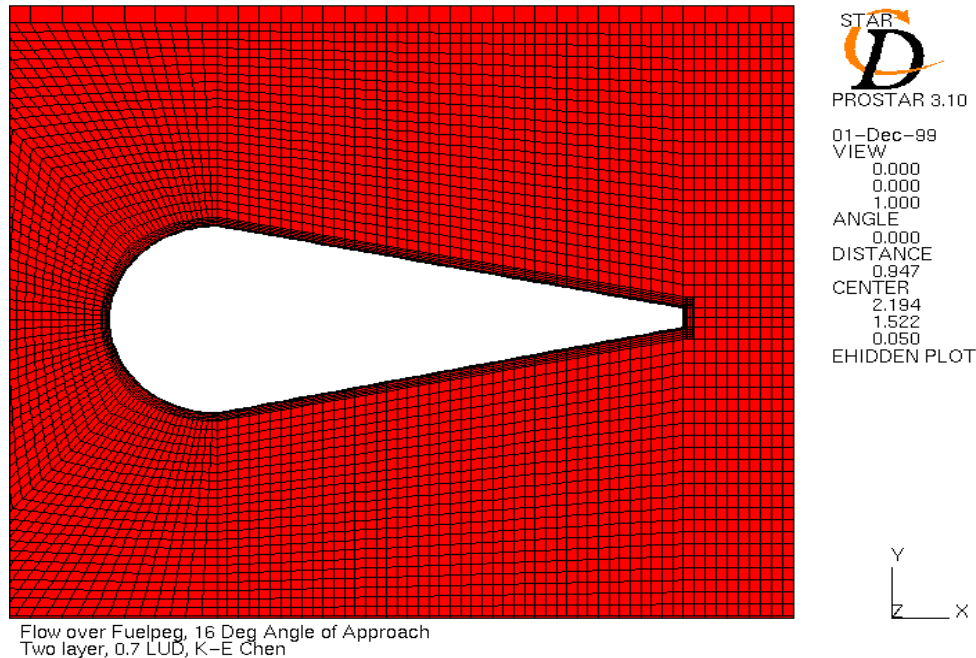


Figure 7.1.1 -- Baseline Fuel-Peg Geometry and Two-Layer Computational Grid

The currently designed fuel pegs work well for fuel injection. However, the blunt upstream surface, the sharp transition from round to flat side surface, and the flat sides of the faring could allow a recirculation zone to form. The recirculation zone *per se* is not a problem. However, a recirculation zone in an area containing a combustible mixture could act as a flame-holder if ignited.

The current fuel peg design has the general shape of an airfoil. However, airfoils, as used on airplane wings, are specially designed so as to minimize formation of recirculation zones. An airfoil must allow flow over both the top and bottom surfaces at a range of angles of approach without forming recirculation zones. As the approach angle is increased, the surface area on the top of the wing is increased. Thus the air velocity is increased compared to the bottom velocity, and lift is generated. Recirculation zones increase drag, and if sufficiently severe, result in the loss of lift (stall). Therefore, an airfoil design has been investigated as an alternate shape for the fuel peg that would decrease the possibility for setting up recirculation zones. Constraints inherent in the design of the fuel pegs include:

- Gas velocity through the fuel peg should be less than 100 feet/sec.
- Pressure drop across the fuel peg fuel jets of approximately 10%.
- Location and orientation of the fuel pegs and lobed mixer must be compatible with the existing Xonon® 1 combustor.

7.2 Airfoil Design

Airfoil design can be very complex, especially for modern planes. However, a lot of research on airfoil design for lower speed (propeller powered aircraft) was performed in the 1940's. This

research is tabulated in Abbott and von Doenhoff, Theory of Wing Sections, 1949. A fuel peg needs to be symmetrical, whereas most wings are not symmetrical having more surface area on the top than on the bottom. The type of airfoil selected for investigation was the NACA00nn airfoil. The “00” indicates that the airfoil shape is symmetrical. The “nn” indicates the airfoil maximum thickness as a percentage of the chord length.

The cross section of the NACA four digit airfoils can be generated from the same equation, which represents the airfoil thickness (y) as a function of chord length (x). The formula was placed into an Excel spreadsheet and was used to generate vertex locations of the bottom ($y = -F(x)$) and top ($y = F(x)$) of the fuel peg/airfoil. These vertex positions were copied to a text file and read into ProStar. A second equation can be used to provide a radius (if needed) to smooth the front edge of the airfoil. The cubic spline algorithm used by ProStar provides an alternate smoothing method. This method was used to complete the model cross section generation. A typical cross section can be seen in Figure C2.

7.3 CFD Model

For the computational mesh, the dimensions of the proposed fuel peg were entered into ProStar as a 2-dimensional geometry. The 2-dimensional model is really 1 cell thick in the z-direction. Note that plots of CFD results are usually constructed normal to the z-axis, so this thickness is not seen, with the exception of y^+ plots.

The base case fuel peg design was based upon a prior CESI design. This design consists of a circular S/S tube approximately 0.5” O.D. A triangular shaped faring is attached to the downstream side of the tube. The model domain consists of a two-dimensional cross-section of the fuel peg located in a rectangular area 3” wide by 10” long. A symmetry boundary is used for the front and back faces of the single cell thick model. These faces are shown as “into” and “out of” the plots, and are not normally seen. Cyclic boundaries are used on the side boundaries. This is the most suitable boundary type (without extending the boundary outward until a stagnation boundary could be used).

Initially, several turbulence models were used, including the κ - ϵ model, the κ - ϵ quadratic model and a κ - ϵ cubic model (under v3.100). It was found that flow separation could be achieved, however, the angle of approach at which flow separation occurred was much higher than indicated from airfoil data (Abbott and Von Doenhoff). After discussions with CSE, it was concluded that none of the available turbulence models were adequate to predict flow separation under these conditions. Therefore, a two-layer model was required.

In the STAR-CD two-layer models, walls requiring additional flow resolution in the near-wall layer are identified. The cells adjacent to the walls are isolated, and successive refinements are made in the direction normal to the wall. A separate turbulence model is used for this near-wall boundary layer. General guidelines are given such that the dimensionless y^+ term should be in the order of 1 at the wall, and that approximately 10 to 15 layers of cells should be included by the code in the near-wall layer. Since these values are not known prior to the calculations, some trial and error is involved.

The baseline fuel peg was modeled first. A “C-mesh” was used to fit around the fuel peg with a minimum number of area intersections on the surface of the grid. The C-mesh was an ideal choice for the two-layer model approach used by STAR-CD. The layer of cells near the wall of the fuel peg was isolated and refined by a factor of about 5 in only the direction normal to the surface of the fuel peg. This process was repeated two additional times so that the cell thickness adjacent to the fuel peg was about 1/125 the thickness of other cells in the same region. This type of refinement provided the desired wall layer thickness as shown by plots of fuel peg wall y^+ and by the number of cell layers used by Star-CD in the near-wall calculations. The same procedure was used to generate wall layers for the NACA00nn airfoil simulations. Typical plots of y^+ and the near-wall cells used by Star-CD are shown in Figures C3 and C4.

The baseline fuel peg and each of the airfoil design fuel pegs were modeled under the same conditions, as summarized in Table 7.3.1. Each fuel peg was initially modeled with air entering at a 0° angle of approach at 14 m/s. The converged result from each run was used as an initial condition for the next simulation, which was ran at a larger angle of approach. The approach velocity was held constant, and only the approach angle changed. This technique could present problems to the model due to the small model domain if either symmetry or stagnation boundary conditions were used. However, the cyclic boundary condition provided a good solution because the flow and angle “out” of one side was matched by the flow and angle “into” the opposite side of the computational grid. (These edges are located along the top and bottom sides of the fuel peg plots.)

Fluid Properties	Air
Equation of State	Ideal Gas (MW 28.96)
Molecular Viscosity	Constant (1.81E-5 kg/ms)
Specific Heat	Constant (1006 J/kgK)
Thermal Conductivity	Constant (0.02637 W/mK)
Exit Pressure	9.E+5 Pa
Turbulence Model	κ - ϵ verX/
Two-Layer Model	Norris and Reynolds
Inlet	
Temperature	750 K
Density	4.237 kg/m ³
Kappa, κ	2
Epsilon, ϵ	80
Solution	
Solution Algorithm	SIMPLE (steady state)
Equation Method	MARS – 0.5 compression
Under-relaxation	0.7 U, V, κ , ϵ ; 0.1 P

Table 7.3.1 -- Fuel-Peg Model Conditions and Methods

7.4 Baseline Fuel Peg CFD

The baseline fuel peg was the first modeled. The fuel peg dimensions were based upon a preliminary design of a combined lobed mixer/ fuel injection system. This system incorporates a 12-lobe mixer with a corresponding 12 fuel-peg, natural gas injection system. The cross-section of the baseline fuel peg is shown in Figure C1. The general outline of the fuel peg is designed to be similar to an airfoil. If a cylindrical tube were used for fuel injection, there would be a major recirculation zone immediately downstream of the tube. This has been significantly reduced through the design of a triangular faring shape attached to the downstream side of the fuel injection tube.

However, the fuel peg design still has some properties that are not ideal from aerodynamic principles. The upstream cylindrical face is relatively blunt compared to the more elliptical shape of the leading edge of airfoils. This produces more flow disturbance and a larger stagnation area at the intersection with the flowing fluid. The transition from the cylindrical leading edge to the flat walls of the faring is very sharp, thus presenting a “tendency” for high velocities to form outwardly directed from the edge of the cylinder. An airfoil has a much smoother transition (i.e., no sharp transition between widening and narrowing sections or continuous first derivative) with the flow tending to bend over the upper section. Minimum flow separation is needed to achieve maximum lift with minimum drag.

The fuel peg CFD model was performed with a cross-section of the outer surface of the currently designed fuel peg. It should be noted that this design incorporates a blunt, flat surface at the trailing edge. This surface is .064” wide and was included with the possibility of injecting the fuel directly downstream. In all of the CFD runs, this flat trailing edge surface caused a local recirculation zone to form. This recirculation would occur with any finite thickness, blunt trailing edge if the computational mesh were sufficiently refined. As this was not the type (or size) of recirculation zone of concern for flame holding (and could be eliminated by extending the faring to a sharp edge), it will not be discussed further.

For all of the fuel pegs modeled, an initial case was calculated with a zero degree approach angle (angle of attack). The second case was calculated using a 5° approach angle with the 0° result as the starting condition. This was repeated for a 10° approach angle. From 10° to 18,° the process was repeated in 2° increments. This information is summarized in Table 7.4.1.

<u>Approach Angle, degrees</u>	<u>U velocity, m/s</u>	<u>V velocity, m/s</u>
0	14	0
5	13.95	1.22
10	13.79	2.43
12	13.69	2.91
14	13.58	3.39
16	13.46	3.86
18	13.31	4.33

Table 7.4.1 -- Approach Angles and Velocity Components

The baseline fuel peg showed one result that did not appear in any of the airfoil calculations. At a very distinct angle, the solution failed to converge. For the CFD modeling parameters listed, the calculations converged at 12° and 12.5°, but failed to converge at a 13° angle of approach. Plots of the U velocity magnitude (see Note 1) at 12.5° and 13° are shown in Figures C5 and C6. Note that Figure C6 was generated after 1000 iterations, but the solution did not converge. This indicates that the baseline fuel peg is stable for flows up to a certain angle, and then abruptly develops a very large and strong recirculation zone as indicated in Figure C6. The steady state solution did not converge because the vortices generated by this large turbulent eddy were continuously being shed, thus there was no steady state solution.

As a numerical experiment, the computational scheme for the baseline case was changed from MARS to LUD. Both models have second order accuracy with respect to the truncation error involved in the numerical approximation of the partial derivatives. The MARS scheme is reported to be the most accurate scheme available within STAR-CD. The LUD model converged at higher approach angles, but also showed the same sudden formation of a recirculation zone with a small change in angle. This behavior is not desirable since it yields a condition where flow disturbances above a certain distinct level would result in a recirculation zone that could act as a flame-holder. This indicates that a design not having this feature would be preferable.

7.5 Airfoil CFD Models

The baseline fuel peg has a thickness to length ratio of 0.375, which would match the thickness to chord length of a NASA0037 airfoil. For a given chord length and “shape”, as an airfoil’s thickness is increased so is the tendency for flow separation. Therefore, airfoil shapes used covered the range of 0.27 to 0.36 corresponding to NACA0027 to NACA0036 in 3% increments. The current fuel peg length of 1.385” was held constant for all runs, with only the thickness varying. All cases indicated by Figure numbers in Table 7.5.1 were run, and the indicated Figures are the representative plots in Appendix C.

Airfoil	10°	12°	14°	16°	18°
NACA0027			Figure C7		Figure C8
NACA0030			Figure C9		Figure C10
NACA0033		Figure C11		Figure C12	
NACA0036	Figure C13		Figure C14		

Table 7.5.1 -- Airfoil Fuel Peg CFD Simulations Approach Angle and Figure Numbers

Two figures have been selected for each airfoil. While certainly some subjectivity is involved, for each airfoil the lower approach angle figure represents a “good”, low recirculation flow. The higher approach angle figure represents a point where the recirculation becomes “marginal”. None of these designs showed a sharp transition angle between low and high recirculation zones as did the baseline fuel peg.

7.6 Conclusions and Recommendations

The conclusion reached from this analysis is that the best choice for the shape of an airfoil fuel peg is the shape of an NACA0030. However, the flow area for natural gas through the fuel-peg decreases as the fuel peg thickness is decreased. As the area is decreased the gas velocity through the fuel peg increases. If the NACA0030 airfoil design would require a maximum gas velocity above 100 fps, then the NACA0033 airfoil is an acceptable compromise.

VIII. Cold Flow Testing of Premixer

8.1 Introduction

The purpose of the Lobed Mixer Cold Flow rig test was to characterize the mixing capabilities of a twelve-lobe mixer developed from CFD analysis in a cold-flow test facility. This facility allows operation at conditions scaled from the Xonon® 1 combustor flow-path. The velocity vectors will be measured with a wedge probe. A mixture of natural gas and air will be injected through the fuel pegs, and the fuel concentrations measured upstream of the simulated catalyst will be used to determine uniformity of fuel and air mixing.

The lobed mixer design has been developed for possible use in the Xonon®1 combustor flow-path. The lobed mixer is an axial flow mixer, as contrasted to the radial mixers used in current CESI designs including Xonon® 2 and Xonon® 2.1. The mixer was designed using CFD simulations as described in the previous section. A solid model image of the mixer and fuel pegs is shown in Figure D1. (Figures for Section 8 can be found in Appendix D) A separate CFD model was used to redesign the fuel pegs for use with this (or other) mixers. The airfoil-shaped fuel pegs were shown to be less susceptible to recirculation and possible flameholding.

8.2 Test Setup / Procedure

8.2.1 Hardware

Figure D1 is a depiction of the lobed mixer to be tested. The unit consists of the lobed aerodynamic piece attached to a combined strut support/fuel injector part. The radial struts will support the unit in the cold-flow rig. Figure D2 shows a notional cross-section of the lobed mixer installed in the cold-flow rig. The mixer is to be installed in the same manner as the old annular-venturi fuel injector. Fuel will be supplied to the central hub and out to the radial struts, where they will be injected through holes upstream of the lobe. The catalyst inlet is simulated with a round perforated sheet.

The fuel pegs to be tested have a cross section based upon airfoil design discussed in the previous Section. CFD modeling has shown that this design shows significantly more resistance to flow separation than the “standard” design currently being used. This resistance to separation at higher approach angles indicates that the fuel peg will be less likely to act as a flameholder. The location and size of holes to be drilled in the airfoil shaped fuel pegs are shown in Table 8.2.1.1.

Number of holes	Distance from edge (2.5" from centerline)	Distance from centerline (inch)	Hole diameter (inch)	Calculated penetration (inch)
2	0.5	3	0.04	1.7
2	1.375	3.875	0.042	1.6
2	2.125	4.625	0.042	1.4
2	2.75	5.25	0.048	1.4
2	3.375	5.875	0.052	1.3

Table 8.2.1.1 -- Location and size of holes to be drilled in fuel pegs

8.2.2 Test Setup - Instrumentation

Figure D3 shows the overall rig instrumentation. Three types of instruments are shown. The first is a series of static wall pressure taps, which are 1/16" stainless-steel tubes, mounted flush with the inside of the wall where the static pressure is being measured. For the three taps shown upstream of the lobed mixer the exact location is not critical - the first will be placed in the inlet plenum of the preburner, the second, halfway along the vertical length of the 'dome' section, and the third, approximately 1" upstream of the lobed mixer. The series of taps downstream of the lobed mixer should be spaced 1.5" apart, with the first one installed 1" downstream of the lobe and the last ending up just upstream of the simulated catalyst inlet (the spacing of the last tap can be adjusted to achieve this).

The second set of instrumentation, shown in the figure, are openings for wedge probe testing. Four locations should be installed. The first three will be installed 1" downstream of the lobed mixer. The circumferential location of these with respect to the rig is not important, but their position relative to the lobed mixer is, and is illustrated by Figure D4. One probe should be placed within an 'outer' lobe, one within an 'inner' lobe, and one across a probe wall. The fourth probe should be installed 7" below the lobed mixer.

The third group of instrumentation will be a fuel/air sampling grid, which will be 1/8" tubes placed in a prescribe pattern on the perforated plate which simulates the catalyst inlet. The tubes may be either plastic or Teflon.

Figure D5 illustrates the pattern to be installed on the perforated plate, while Table 8.2.2.1 lists the radial and circumferential position for each sampling tube. Of the 72 channels available on the test rig valve system, 68 will be used for fuel/air sampling, two for sampling of the inlet air flow, and two will be spare.

Sample Point #	Radii	Angle	Sample Point #	Radii	Angle
1	1.5	0	41	6.5	15
2	1.5	90	42	6.5	45
3	1.5	180	43	6.5	75
4	1.5	270	44	6.5	105

5	2.5	45	45	6.5	135
6	2.5	135	46	6.5	165
7	2.5	225	47	6.5	195
8	2.5	315	48	6.5	225
9	3.5	0	49	6.5	255
10	3.5	45	50	6.5	285
11	3.5	90	51	6.5	315
12	3.5	135	52	6.5	345
13	3.5	180	53	7.125	0
14	3.5	225	54	7.125	30
15	3.5	270	55	7.125	60
16	3.5	315	56	7.125	90
17	4.75	15	57	7.125	120
18	4.75	45	58	7.125	150
19	4.75	75	59	7.125	180
20	4.75	105	60	7.125	210
21	4.75	135	61	7.125	240
22	4.75	165	62	7.125	270
23	4.75	195	63	7.125	300
24	4.75	225	64	7.125	330
25	4.75	255	65	7.375	45
26	4.75	285	66	7.375	135
27	4.75	315	67	7.375	225
28	4.75	345	68	7.375	315
29	5.75	0			
30	5.75	30			
31	5.75	60			
32	5.75	90			
33	5.75	120			
34	5.75	150			
35	5.75	180			
36	5.75	210			
37	5.75	240			
38	5.75	270			
39	5.75	300			
40	5.75	330			

Table 8.2.2.1 -- Fuel/Air Sample Point Locations

8.2.3 Summary – Test Run #1

The purpose of this test was to conduct initial cold flow, experimental tests of a twelve-lobed mixer. This mixer is based upon the best of several sine-wave shaped mixing lobes on which CFD simulations were performed. As no prior lobed mixers have been tested, no data is

available for comparison. However, the same methodology is used as has been used to test radial mixers.

Figure D5 shows a cross-sectional plot of sampling locations, with the 0° location located at top dead center. The fuel pegs are shown by the magenta lines at 0°, 30°, up to 330°. The fuel pegs are located midway between the inner and outer directed lobes. The fuel pegs are symmetric, so the central angles between fuel pegs represent lines at which the jets from the fuel pegs collide.

Figure D6 shows a plot of the Hydrocarbons (Natural Gas) concentration in ppm versus location. Note that there is a decrease in HC concentration from the outer sampling points toward the innermost sampling points. This concentration gradient is seen around the full 360° cylindrical cross-section. The concentration varies from 650 ppm at the center to 1075 ppm at the outer edges. The average concentration is 930 ppm, giving a maximum of +16% and a minimum level of -30%. This non-uniformity is greater than would be acceptable for use in a catalytic combustor. However, the inner to outer gradient can be relatively easily adjusted by modifying the size and/or location of the fuel injection points. This would provide more fuel to the low concentration center and/or less to the higher concentration outside.

Figure D7 shows a plot of all of the sampled data points plotted as deviation from average versus radial distance from the center. This plot shows the overall concentration gradient from low on the inside to high on the outside, as noted above.

Figure D8 shows a plot of all sampled points deviation plotted versus angle. This figure shows that there is some concentration gradient with angle. Measurements taken between 90° and 270° show lower concentrations than measurements taken at other angles. It is believed that this is probably due to a slight misalignment of the center-body and/or test piece. This gradient should be easy to remove.

It should also be noted on Figure D8 that all of the “lowest” points (greatest negative deviation from average) are from the innermost two diameter sampling points. This corresponds to the observation that the lowest concentration occurs at the innermost location.

If Figure D6 is studied in detail, there are “lighter” (higher concentration) areas and “darker” (lower concentration) areas around the outer perimeter of the sampling area. Figure D8 shows a plot of the fuel concentrations from the outer two sampling radial sampling points only. It should be noted that the lowest concentrations of fuel occur at angles of 90°, 120°, 180°, 210°, 240° and 270°. From Fig D5, it can be seen that these points are directly downstream of pegs.

8.2.4 Discussion and Conclusions

A significant concentration gradient from the inside to the outside of the sampling system was seen. This can be improved by modification of the hole size, hole number and hole positions on the fuel pegs. The lower concentration seen on one side of the sampling system can also be improved with moderate effort.

The observation that is of most concern is that the lowest concentrations of fuel occurred at angles between 90° and 270° and directly downstream of the fuel pegs. This sector (90° to 270°) is consistent with an overall skew in the flowfield. However, the low concentrations, which match the fuel peg locations, indicate that little mixing is occurring in the circumferential direction. This is one conclusion that was reached as a result of the CFD modeling.

However, it is promising that the low concentrations occur directly downstream of the fuel pegs instead of between the fuel pegs. Since the intermediate angles (105°, 135°, etc.) are not the lowest concentration locations, it is concluded that jet penetration from the fuel pegs is performing as desired. (If the low concentrations were half way between fuel pegs, it would indicate that jet penetration was not adequate. This would require an increased number of fuel pegs, or similar modifications to correct.)

IV. Flameholding Study – UCI, Experimental Analysis

9.1 Background and Introduction

In advanced lean burning gas turbines, obtaining low NO_x levels requires careful premixing of the fuel and air. This is true for both gas phase and catalytic combustion strategies. In conjunction with a requirement for uniform fuel/air mixtures, catalytic combustion also has some requirement relative to velocity profiles entering the catalyst. As a result, the design of the premixer becomes a significant challenge. As combustion system inlet temperatures increase in order to attain higher efficiencies, the likelihood of autoignition in the premixing duct increases. Incorporation of cost effective manufacturing strategies requires additional design considerations regarding the joining of parts. As a result of these requirements and concerns, questions relative to the role of perturbations in the walls associated with joints, protrusions, and fasteners arise. Will these lead to autoignition? If so, will these perturbations hold flame and therefore cause structure damage to the premixer and possibly the engine?

The purpose of the current project is to address these questions. The approach taken is to develop a flow tube which can provide the velocities, temperatures, pressures, and perturbations representative of those found in practical engine applications. Fuel distributions and velocity distributions were measured. A statistically designed experiment was developed and conducted in order to identify the key factors affecting flameholding.

9.2 Literature Review

The literature review indicted that the work of Cambel and co-workers (1957, 1958, and 1962) and that by Ballal and Levebvre (1979) were the only highly relevant prior studies. A lack of correspondence to the results of Cambel and co-workers was found and is attributed to a lack of consideration for pressure and temperatures effects in the prior work. However, the study of Ballal and Levebvre (1979) appears to describe the flameholding tendencies reasonably well despite the fundamental differences in the geometries considered. The present study examined much smaller perturbations compared to those of Ballal and Lefebvre. The focus on relatively small perturbations allowed additional conclusions to be drawn. The mechanism for flameholding appears to exhibit a sharp transition that occurs for step expansions between 0.125”

and 0.0375.” Further, it is reasonable to avoid flameholding for the conditions considered by using perturbations, which are 0.0375” and less. Velocity and pressure were found have the greatest affect on WE (weak extinction) limits. This could be due to the relatively narrow range of temperatures studied. In general, higher pressures, higher temperatures, and lower velocities lead to lower WE limits, though the effect of velocity was found to depend upon the pressure. In particular, velocity effects are diminished at lower pressures.

The aim of this study is to obtain a fundamental understanding of the mechanisms of flameholding in fuel/air premixing passages for advanced lean burn gas turbine concepts. In such systems, there is a risk of autoignition, flashback, and flameholding within the premixing passage. This particular study examines the effects of geometric disturbances in the flow path on the flameholding potential of the premix passage.

9.3 Experimental Apparatus

The design and fabrication of a semi-independent test rig to provide an experimental model of a lean burn fuel/air premixing passage comprised a significant portion of the overall effort. While the vessel is self-contained, it relies upon facility supplied preheated air and cooled exhaust capabilities for operation.

9.3.1 Test Conditions

In order to simulate the environment of a premixing passage for a natural gas fired gas turbine, both high pressures and high temperatures are required. To generate these conditions the UCICL High Pressure Facility is employed. The facility is capable of generating a preheated airflow at temperatures up to 1200 F and at pressures exceeding ten atmospheres. The maximum flow rate from the facility exceeds 3 lb/sec. Conditions for the experiment are listed in Table E1. (NOTE: All Tables and Figures referenced in Section 9 can be found in Appendix E).

In addition to the listed flow conditions there are geometric conditions for the experiment listed in Table E2. It is noted that, although the geometries were fabricated, the emphasis for the current phase of testing was directed at the sudden expansion type geometries. This was felt to (1) provide the most likely scenario for flameholding, and (2) provide the closest approximation to the type of perturbations found along the walls in practical premixing devices for a variety of manufacturing approaches. The facility was designed, however, to allow the additional parametric geometries to be evaluated.

9.3.2 Hardware

The hardware setup for the experiment can be broken down in to three major sections:

1. Inlet/Conditioning
2. Test Section
3. Exhaust/Cooling

Each section is described briefly in the following sections. Figure E1 illustrates the overall schematic of the experimental apparatus.

Inlet/Conditioning:

The individual components for the inlet and conditioning section are:

1. Four inch to two-inch reducer
2. Two-inch steel braided hose
3. Flow conditioner
4. Transition
5. Natural gas injectors
6. Mixing length
7. Turbulence intensity grid

The existing facility connection for the preheated airflow is a four-inch, 600-lb ANSI standard flange fitting. This fitting is reduced to a two inch, 600-lb flange fitting to more closely match the premixing duct dimensions. Connection to the test rig is made by a two-inch steel braided flex hose, which joins the reduced facility connection with a flow conditioner (Vortab). The flow conditioner serves to provide a uniform velocity profile upstream of the natural gas injectors and test section. The next section makes a transition from the circular cross-section of the flow conditioner to the semi-square cross-section of the premixing passage. At this point natural gas is injected axially with the flow stream. Finally, a 12-inch mixing length provides some time for mixing of the gas before entering the test section. It is within this mixing length that upstream pressure readings of the vessel are taken. A turbulence grid can be added immediately upstream of the fuel injection section. Actual turbulence levels are determined by laser anemometry. All connections between individual components are made by 600-lb flange connections. The gaskets between connections upstream of the flow conditioner are ceramic filled, wire wound gaskets. Gaskets downstream of the flow conditioner are self-energizing metallic ring seals. These special seals are used in order to eliminate the gap between components that a normal wire wound gasket would create. By eliminating the gaps a more uniform flow condition at the inlet to the test section is provided. Additionally, the gaps would be a possible location for flameholding upstream of the test section. Figure E3 presents a photograph of the inlet/mixing section with the various key components identified. Flow is moving from the right to left in this photograph.

Test Section:

The individual components in this section are:

1. Main Block
2. Hydrogen Igniter
3. Three-inch windows
4. One-inch window
5. Step Insert

The main block is shown schematically in Figure E4. The flow enters from left from the conditioning section. A typical step insert is shown positioned below the test section. The round optical ports are visible on the sides of the schematic. Figure E5 presents a photograph of the test section with some of the key features pointed out. The larger windows shown are utilized to visualize the ignition process and to provide optical access for the measurement of the main stream velocity profiles using laser anemometry. Figure E6 presents a detailed schematic drawing of the test section for additional reference.

The main block of the test section provides pressure and flow constraint as well as providing mounting locations for the other components. The hydrogen igniter, provided by CESI, injects a premixed hydrogen/air flame into the test section. Ignition is upstream of the geometric disturbance and is termed “soft ignition”. This method of ignition is used, as it is considered more representative of actual autoignition conditions in a premixing passage. A premixed hydrogen flame is used to ensure full penetration and, therefore, complete ignition across the cross-sectional area of the premix duct. It is important to have complete ignition so as to ensure that high-energy radicals reach the geometric disturbance and are not trapped above it in high cross-flow situations. The three-inch windows allow for laser anemometry measurements and visual confirmation of hydrogen igniter operation. A thin piece of ceramic paper is placed between the test section and the window to prevent fracturing of the window from thermal expansion of the metal. Fused quartz is used for these windows due to its high thermal shock resistance. The one-inch window is placed at the geometric disturbance. This provides for visual confirmation of a flameholding situation and helps determine where in the test section the flame has stabilized. Fused quartz is also utilized in the one-inch window for its thermal shock resistance. The geometric disturbance is generated by an insert, which is placed in the test section and creates an expansion, contraction, channel, or transition angle. A thermocouple is placed in the insert to measure temperature at the disturbance providing an indication of flameholding. Finally a thermocouple is placed at the exit of the main block indicating if flameholding is taking place somewhere upstream.

Exhaust/Cooling:

The exhaust and cooling section consists of the following components:

1. Four-inch steel braided hose
2. Water quench body and injectors
3. Four-inch steel braided hose

The exhaust is quenched by a water injection system, which is illustrated in Figure E7. After the flow leaves the main body it passes through a four-inch steel braided hose that connects to the water quench body. The water quench body contains four high-pressure water nozzles that flow in excess of 14 gallons per minute into the exhaust stream. The steam-laden exhaust is then passed to the facility water drop out system through a four-inch steel braided hose.

9.3.3 Data Acquisition

Labview 5.1 from National Instruments is used as the platform for a data acquisition and control program. A “virtual instrument” running in Labview allows the experimenter to collect temperature and pressure data as well as control the hydrogen igniter and natural gas flow. Maximum igniter on time is programmable and a backup solenoid valve actuates to shut off hydrogen flow when this time limit is exceeded. Upstream pressure, exhaust temperature, and step temperature are all recorded in real time using a SCXI system and a sample and hold, differential input amplifier from National Instruments.

The detection of the flameholding was accomplished visually. A small video camera was positioned to view the region from the main view port and the step view port. Flameholding was also monitored by a thermocouple at the step and by the post step thermocouple. The post step thermocouple and the visual indication were relied upon to provide the necessary information.

Fuel Distribution Across the Test Section

The measurement of the fuel distribution was accomplished using a special sampling section installed between the mixing section exit and the test section just for this measurement (it was not in place for the actual flameholding experiments). Nine evenly spaced discrete points (sample probe points) were monitored. The flow from each probe was sequentially fed to a high range FID hydrocarbon analyzer, which measured the concentration at each of the points.

Velocity Distribution Across the Test Section

The measurement of the velocity field within the inlet section was measured using laser anemometry. A two-component fiber optic system was installed onto a traverse system to provide two degrees of freedom. A photograph of the setup is shown in Figure E8. In the foreground is the two-component transceiver unit that serves to create the sample volume where four laser beams intersect as well as to collect the scattered light.

A custom high volume seeding system was developed specifically for this project. It utilizes 1-micron alumina particles that are injected via a slurry solution using a twin-fluid atomization process. With the high preheat provided by the system, the water is easily vaporized, leaving the dry particles which then serve to scatter the laser light.

9.3.4 Prescreening Test Matrix

It was decided to utilize statistically designed experiments to conduct the experiment in the most efficient manner. After review of the possible testing that could be accomplished with the parameters provided in Table E1 and Table E2, it was decided to focus upon the cases with the sudden expansion for the purpose of the present study. This results in a total of 6 parameters for study (expansion height, temperature, pressure, velocity, turbulence, and equivalence ratio. As a result, a 2^6 two-level, full factorial experiment was generated, resulting in 64 total cases. In addition, 5 center points were added to assess pure error and curvature in the response. The resulting planned matrix is shown in Table E3.

The matrix shown in Table E3 was also utilized to assess the likelihood that flameholding would be observed for at least some of the geometries and conditions considered. This is typically accomplished by prescreening experimentally. In the present case, Equation 1 was applied to the conditions listed in Table E3 and utilized to generate the expected equivalence ratio at which flame holding would result.

The conclusion from Ballal and Lefebvre (1979) is summarized by the following correlation, which expresses the weak extinction limit as a function of various parameters:

$$\phi_{LBO} = \left\{ \frac{2.25[1 + 0.4U(1 + Tu')]}{P^{0.25} T_o e^{(T_o/150)} D_c (1 - B_g)} \right\}^{0.16} \quad \text{Equation 1}$$

where

- U is the mainstream velocity, m/s
- T is the mainstream temperature, K
- u' is the mainstream fluctuating velocity, m/s
- P is the pressure, Pa
- T_o is the mainstream temperature, K

D_c is the characteristic dimension, m

B_g is blockage ratio (flameholder area to main flow channel area)

These predictions are presented in Figure E9. The results indicates that, for the conditions illustrated in Table E3, a significant number of cases should experience flameholding, thereby helping to verify that the range of conditions was suitable for the present study (i.e., serving as “pre-screening”).

Upon the conduct of shakedown testing, the “design space” (i.e., the limits in the ranges for each parameter) was modified somewhat. This is reflected in the presentation of Table E1. As a result, the planned matrix presented in Table E3 was not fully evaluated. It was found, for example, that the system could not support flow rates in excess of 0.8 lbs/sec at seven atmospheres. Since the limitation affected only two out of 18 tests, the two out of range tests were conducted at lower velocities. Pre-heating was another significant issue. While the facility is capable of heating large flows of air (0.1 to 1.5 lbs/sec), it is not well suited for high preheats of small mass flow rates. This set the low velocity limit at 100 ft/sec to prevent overheating the heater elements.

As a result of the shakedown tests, a new matrix was generated based on the constraints determined. This matrix is presented in Table E4. Note that turbulence intensity was dropped as a parameter.

The first test conducted consisted of “go/no go” type responses for the matrix delineated in Table E4. In order to maximize efficiency, the tests were not conducted in a purely random order. Instead, they were run in the order that was most time efficient. The basic protocol utilized to run the tests was the following:

For any given block, preheat temperature was set first. Pressures were varied for the set temperature. Velocities were varied for a given pressure. And finally, equivalence ratio was adjusted for a specific velocity. Table E5 provides an example of the order for which testing was conducted for one of the blocks, which prove to be the most efficient time wise.

For cases where flameholding was observed at only the higher equivalence ratio, additional time was taken to establish the approximate value for the equivalence ratio where flameholding initiated. These results could then be utilized to compare with the previous studies of Choudhury and Cambel (1962) and Ballal and Lefebvre (1979).

9.4 Results

9.4.1 Observations and Anomalies

Positive and negative results were determined visually. Figure E10 shows the initial step in a reacting test. The blue flame upstream originates from the hydrogen igniter. Downstream an orange glow emanates from the step disturbance. In the second phase of the test, the igniter is shut off and determination of flameholding is made. Figure E11 shows two cases where positive flameholding was observed. In case ‘a’ the flameholding is very bright and intense.

Case ‘b’ also shows a stabilized flame but at a much lower intensity. Flow conditions as well as step geometry are believed to determine the intensity of the flame.

Some anomalies were observed during testing. The most prevalent of these was flameholding upstream of the step. The test section introduces small disturbances upstream of the step. Two of the most notable disturbances are at the igniter end and at the window interface to the cross-section. During some tests the flame held at these disturbances. If the flame was determined to be holding upstream, the test was disregarded and rerun until the flame blew off of any point upstream of the step. Example images associated with flameholding at the igniter and at the window are shown in Figure E12.

Another anomaly that was observed was the fluctuation of the system pressure controller. For a set system pressure, the controller indicated an oscillating pressure. At 7 atm the average deviation was 2% of the mean. At 2 atm the deviation was roughly 4%.

Additional observations were made throughout the course of testing which are noted here as part of the screening results.

- Low air speeds of about 20 ft/s, especially when combined with high equivalence ratios, lead to a detonation in the vessel.
- Preheated air-flows should be greater than 0.1 lbs/sec to avoid low flow shut off of the heaters. This is an issue associated with limitations of the facility.
- Higher air-flow rates create a minimum static pressure in the vessel. This should be less than 14 psig for flows less than 1.2 lbs/sec. Again, this aspect is specific to the current facility.
- The hydrogen igniter does not fully penetrate the stream for high flow speeds. It does, however, seem to propagate across the tube by the time it reaches the step.
- There is a transition range for varying equivalence ratios such that a flame will hold strongly at a high ER, blow out at low ER, and hold with instability at median ratios.

9.4.2 Velocity Distribution

Velocity measurements were obtained using laser anemometry as described in Section 9.3. The results were obtained for a 5 x 5 evenly spaced grid with a distance of 0.25” from the inner surfaces maintained. In terms of the orientation, the reference location is the lower left corner of the cross flow section when viewed from aft looking forward towards the inlet.

Results were taken for four representative conditions featuring extremes in both velocity and pressure. The results obtained are shown in contour form in Figure E13 for the selected conditions. The same results are presented in Figure E14 in the form of % deviation from the mean velocity:

$$\%Dev = \frac{(U_i - \bar{U})}{\bar{U}} \cdot 100 \quad \text{Equation 2}$$

To facilitate the interpretation of the mean velocity field, Figure E15 presents the same results plotted in a surface map form. Note that there are five fuel injection ports, which were operated with natural gas during the velocity measurements at flow rates corresponding to a phi of 0.6.

For reference, five injection points are utilized located an evenly spaced quadrants and a single centerline injection points.

The mean velocity fields do exhibit some variation. This may be due, in part, to the operation of the natural gas injector, or to variations in the total flow rate. For low flow rates, in particular, the test facility sustained a slowly varying oscillation in flow due to the controller. As a result, more confidence is placed in the high velocity cases.

Typical flow oscillation in the combustion air mass flow controller was ± 0.02 lb/s. This was accompanied by variations in the natural gas controller on the order of ± 2 psi. Based on these variations, the equivalence ratio was found to vary by as much as 17% for very low flows (e.g. < 0.12 lb/s of air) and as much as 2.6% for high flow rates (e.g. ~ 1.00 lb/s of air). Additionally, variations in the air-flow rate and pressure affect the velocity through the test section. The pressure variation is mentioned in Section 4 but does not exceed 4%. This pressure variation coupled with the variations of the air-flow rate and the natural gas composition leads to a maximum velocity deviation of 6%. All of the aforementioned variation levels refer to the total system conditions and do not address local flow conditions in the test section. Development of the flow, turbulence, mixing, and general flow instabilities all affect local conditions.

9.4.3 Turbulence Intensity

In order to ascertain the turbulence levels within the test section, the fluctuating velocity associated with the streamwise component (axial) was quantified by the rms (root-mean-square) of the distribution about the mean. The turbulence intensity is this value divided by the mean velocity at that point. The results are presented in Figure E16. In addition, the overall average turbulence intensity is provided in the legend at the top of each contour plot. For the baseline case, the average turbulence levels were approximately 7% for each case studied. Note the presence of fairly high turbulence regions in some of the corner regions of the test section.

As part of the program, it was desired to vary the turbulence intensity to determine the impact of this parameter on the flameholding characteristics. Armed with the results presented in Figure E16, the task of changing the turbulence level was undertaken. The original plan called for the insertion of grids into the flowfield to either reduce or increase the turbulence based upon the natural turbulence generated by the baseline system. The relatively low turbulence levels found in the baseline configuration, suggested that increasing the level would be the best approach. Several methods were tried in order to accomplish this goal. Initially, three $1/8$ " rods were placed across the duct. The new measured turbulence intensities were within 1% of baseline conditions. Next, a pair of $1/2$ " tubes was inserted across the duct, downstream of the $1/8$ " rods, in an orientation perpendicular to the smaller rods. Despite the relatively high blockage ratio introduced by the $1/2$ " tubes, there was no measurable effect on the turbulence intensity. The section that contains the turbulence grid was also turned 45 degrees about the longitudinal axis (i.e. the flow axial direction). This prevented the sections from aligning properly, thereby creating major disturbances at the walls. Again, very little effect was seen on the baseline turbulence intensity. The only method that produced significant changes in baseline turbulence levels was the use of a "V" gutter placed just upstream of the test section. Intensity levels varied from 29% to 48%. Ultimately, the method that produced significant variations in turbulence also distorted the velocity profile so dramatically that the velocity at the step disturbance would be

unknown or have very large errors associated with it. Figure E17 shows the turbulence intensity and velocity contours for the “V” gutter arrangement. Average turbulence intensity was 38.9%.

9.4.4 Fuel Distribution

Measurements of the fuel distribution for the same four conditions for which velocity measurements were obtained are presented in Figure E18. The results illustrate some non-uniformity in the fuel distribution. This is attributed to a combination of the velocity field and fuel injection manifold. The details of the design indicate the path length to the lower injection points is indeed longer than that to other points. However, the fuel concentration at the lower boundary is the critical value since the flameholding step is oriented at the bottom of the channel.

9.4.5 Flameholding Results

As alluded to previously, the planned 2^6 factorial test matrix was not fully executed. This was due to inability to generate sufficient differences in turbulence. As a result, a sub-matrix was executed, consisting of a single turbulence level. As a result, the basic test plan was reduced to a 2^5 factorial (temperature, pressure, step height, equivalence ratio, velocity), with some centerpoints.

The observed flameholding results are presented in Table E5. In the “result” column, most of the cases have a weak extinction limit listed. For these cases, flame holding was observed above or at this limit but not below this limit. Some cases do not have a weak extinction limit listed. This is due to the configuration failing to hold a flame at an equivalence ratio of less than or equal to 1.0. Since the results presented in Figure E18 revealed variation in the fuel distribution, the detailed measurements were evaluated and it was concluded that the equivalence ratio near the step was approximately 70% of the overall equivalence ratio. As a result, a “corrected measured WE limit” is also presented in Table E6, which is simply 70% of the actual overall average. Table E6 also has a column for repeated measurements. These results were obtained several weeks apart with substantial tear down of the facility in between. As a result, they provide a good indicator of the repeatability of the testing procedure and results.

9.5 Discussion

For the results obtained where the weak equivalence ratio was identified, comparison to the work of Cambel and Ballal and Levebvre can be made. Figure E20 provides a comparison of the uncorrected results with the work of Cambel. The general trends from the present study match those established by Cambel, who did not study the effects of temperature or pressure on the flameholding tendencies. However, the results from the present study indicate a much broader variation in equivalence ratio compared to the prior work. This is attributed to the additional parameters studied as well as apparent “regime” behavior with respect to step height. As a result, the correlations from Cambel are inadequate for the present case and additional analyses are required. If the corrected values are utilized in place of the uncorrected values, the results would be shifted to even leaner levels.

Additional comparison can be made with Ballal and Lefebvre (1979). The comparison is presented in Figure E21 for the uncorrected measured WE values. The general trends shown in

Figure E21 do appear better behaved compared to those illustrated in Figure E20, suggesting that a more comprehensive correlation does a much better job in explaining the behavior. It is noted that the behavior for the 0.25” step expansion appears better described by the correlation than does the smaller step. Indeed, flameholding was rarely, if at all seen for the 0.0375” step (see Table E6), suggesting that a certain “critical” step expansion may be required to allow flameholding at all. This is further suggested by the strong co-mingling of results from the 0.25” and 0.125” step in Figure E21. No clear trend is evident for step height, other than the implication that once the step gets to be 0.125”, flameholding is likely to occur for some operating conditions.

The trend predicted by Ballal and Lefebvre is consistently leaner than that found in the present study, but the current values of WE are consistently higher. Because of the relatively non-uniform fuel concentration, it was decided to examine how well the predicted WE limits compared to the measured values based on the local equivalence ratio. Examination of the results shown in Figure E18 suggested that the actual equivalence ratio in the region near the step expansion was about 70% of the overall average equivalence ratio. As a result, the correlation was reanalyzed using the corrected values. The results are shown in Figure E22 and it appears that the Ballal and Lefebvre (1979) model does a reasonable job in predicting the behavior, especially for the 0.25” step expansion.

Because the data were obtained following a statistically designed experiment, the results were examined using analysis of variance. The results shown in Table E6 were analyzed in this manner using Design-Expert 6.0 (Stat-Ease, Inc.), including the repeated points shown. The results are shown in Figure E23 and Figure E24. The only difference between the analyses is the purposeful inclusion of temperature in Model B. Note that, in both models, step height is not found to be significant. In the analysis, the smallest step height was set at 0.125 since flameholding was not typically detected with the shorter step expansion. The main effects include an interaction between pressure and velocity. At higher pressures, velocity plays a more important role according to the results obtained.

Because of the expected role of temperature, another analysis was conducted where temperature was purposefully included in the regression model. These results are presented in Figure E24. The results do not change significantly.

In the case of Model A, Equation 3 is an expression for weak extinction:

$$WE = 0.7847 - 0.088 * Pressure - 0.00006258 * Velocity + 0.00058 * Pressure * Velocity$$

Equation 3

However, while the F-Value associated with the model is 9.56, indicating a significant model, significant lack of fit is also noted (F-Value of 33.64). In the case of Model B, Equation 4 describes the weak extinction limit.

$$WE = 0.99 - 0.00017 * Temp - 0.091 * Pressure - 0.0013 * Velocity + 0.0006 * Pressure * Velocity$$

Equation 4

Model B is again found to be significant, but again with lack of fit. Additional terms could be added to the model, but the results do not improve significantly. As a result, it might be concluded that the effects are highly non-linear. Since the smallest step did not hold flame, centerpoints were not available with which to check for curvature. However, in both cases, the pure error associated with the three repeated points was very small compared to the main effects.

To further summarize the results in a visual manner, a color-coded version of the results for the 0.25" step is presented in Figure E25. These results illustrate some inconsistency in the trends (especially at the 5.5 atm condition). And perhaps these inconsistent points should be discounted in the ANOVA. For now, however, they are included because of the repeatability demonstrated.

9.6 Summary, Conclusions, and Recommendations

9.6.1 Summary

A literature review was conducted in an effort to find comprehensive work, which examined flameholding tendencies of wall perturbations. Several relevant works were found, but in most cases were focused on strategies designed to hold flame rather than examining the limiting cases. A facility was constructed to specifically study flameholding tendencies of wall perturbations as a function of temperature, pressure, flow velocity, turbulence intensity, equivalence ratio, and step geometry. Methodology was included to measure the fuel distribution and velocity distribution within the flow reactor. In the present study, the effect of step expansion was evaluated.

9.6.2 Conclusions

Some general conclusions are:

1. The basic trends observed are consistent with previous studies. However, the results exhibit much broader tendencies compared to the early work of Cambel and co-workers (1957, 1958, 1962) which is attributed to the inclusion of temperature and pressure effects in the present study. The study of Ballal and Levebvre (1979) appears to describe the flameholding tendencies reasonably well. In particular, if the local fuel concentration was considered, the agreement was quite reasonable.
2. Step heights seem to have weak influence on the WE limits of a positive, flameholding case. This is seen in the similar results for the 0.125" and 0.25" step. The mechanism for flameholding appears to exhibit a sharp transition that occurs somewhere between 0.125 and 0.0375" step expansion. Further, it is reasonable to avoid flameholding by using perturbations that are on the order of 0.0375" and less.
3. Velocity and Pressure have the greatest effect on WE limits. The lack of temperature dependency is attributed to the relatively narrow range of temperatures studied.
4. Higher pressures, higher temperatures, and lower velocities lead to lower WE limits, though the effect of velocity was found to depend upon the pressure. In particular, velocity effects are diminished at lower pressures.

9.6.3 Recommendations

Several recommendations for further work include

1. The measured fuel distribution was not as uniform as desired. This was found despite care taken in flow conditioning and fuel injection. Some issues were found to be a result of the square geometry utilized, including corner turbulence generation. As a result, additional effort for flow conditioning is suggested. However, since the profiles were measured for several cases, this can be considered to some extent in the analysis.
2. Since a “regime behavior” was observed for step height, it would be useful to study step height in a more systematic manner (e.g., conduct studies for many step heights between 0.0375” and 0.125”) in order to provide optimal guidance.
3. Other wall geometries should be evaluated (e.g., simulated screw or bolt heads).
4. Comparison to CFD modeling should be conducted to help “fill in” missing information which might then be used to explain the results.

X. Flameholding Study – CSE, Simulation & Analysis

10.1 Introduction

Combustion Science and Engineering, Inc. (CSE) has been tasked by Catalytica Combustion Systems, Inc (CESI) to analyze the differences in two possible experimental geometries that may be used to examine the issue of flameholding in a fuel/air mixing duct. In this report, the CFD modeling performed to determine flow field differences in a 1-inch square duct versus a 2-inch square duct is presented. Additionally, the CFD models were used to determine recirculation times for the region of separated flow directly downstream of the step. The recirculation time was then utilized in a previously developed analytical technique to determine, if predicted recirculation zones or regions of separated flow have flameholding potential. This technique utilizes the CFD flow field predictions as inlet conditions to a Perfectly Stirred Reactor (PSR) model. The PSR model allows for the utilization of a comprehensive, chemical kinetics reaction scheme to predict the potential for flameholding.

10.2 Background

In both lean, premixed combustion and catalytic combustion systems, mixing of the fuel and air is a fundamental issue. In these systems, the ability to rapidly mix the fuel and air is critical. However, premixed fuel and air systems also present the potential for flameholding at locations of separated flow, in cavities or recesses, or in the wake behind bluff bodies. Flameholding in unintended locations can lead to component burnout or damage. The present program examines flameholding within premixer passages from both a computational and experimental perspective.

A number of different geometries and inlet conditions will be used to determine flameholding potential. These conditions will be investigated both computationally and experimentally. The experimental program will provide validation data for the development and refinement of the analytical techniques. This initial computational task will assist in determining the scale of the experimental apparatus required for adequate modeling resolution.

The flameholding potential is determined using a technique developed previously by CSE for CESI [1, ref list at the end of this section]. The present approach uses a perfectly stirred reactor (PSR) model with full chemical kinetics. This approach simplifies the fluid mechanics but eliminates the weakness of one step global kinetics. However, the fluid mechanics is accounted for by using results from CFD modeling to develop the appropriate input parameters for the chemical reactor model.

10.3 CFD Model

The two proposed test sections were modeled using a commercial CFD code, STAR*CD [2]. STAR*CD is a general-purpose CFD code that uses the finite volume method. In this approach, the domain is divided into numerous discrete control volumes, or cells. STAR*CD is capable of analyzing a wide variety of meshes, from completely structured hexahedral meshes to fully unstructured meshes. The mesh can be composed of the usual cell types (e.g. hexahedral, prism, pyramid, and tetrahedral) as well as polyhedral cells. These cell types can exist in the mesh individually or simultaneously in any combination. For this modeling effort, only hexahedral cells were used.

The conservation equations solved in the problem (momentum, mass, energy, etc.) are discretized for each control volume. The derivatives are evaluated with reference to the cell in question and its neighbors. This results in a set of non-linear equations that are solved by iteration. The efforts required to solve these equations are influenced by the number of cells, the number of conservation equations being solved, the type of solver and the computer system being used. STAR*CD has a number of physical and numerical modeling capabilities, which are too numerous to describe adequately in this report.

Both two-dimensional and three-dimensional models were constructed for this study. The three-dimensional models (Figure F1) were used to determine if spanwise flow would greatly affect the recirculation time of the mixing zone. The three-dimensional models consisted of approximately 390,000 cells. The two-dimensional models used symmetry plane boundary conditions in the axial direction, which reduced the number of cells to approximately 15,000. High cell densities were used in regions of interest such as areas of flow separation. A two-layer model [3] was used in the wall region for better resolution and more accurate representation of the boundary layer. Turbulence was modeled using the standard k-e model with and without the Chen's modification for high-shear flows [4].

Per data supplied by CESI, identical inlet conditions were used for both the one-inch and two-inch test sections. The inlet flow velocity was 50 ft/s with a prescribed turbulent intensity of 20%. The pressure and temperature of the model was 9 atm. and 850 °F respectively. The step height was fixed at 0.25 inches for both models. Adequate distance before and after the step was used (and proved necessary) to ensure fully-developed flow at the step and non-separated flow at the exit. Table 10.3.1 contains a summary of the conditions used in the models. The Reynolds' numbers ($Re = V*D/v$) are based on the hydraulic diameter (i.e. $2 * \text{height}$) of the inlet and the aspect ratio is the ratio of the outlet height to the inlet height.

Inlet Conditions

Property	1-inch x 1-inch	2-inch x 2-inch
Velocity (ft/s)	50	50
Turbulent Intensity	20%	20%
Pressure (atm)	9	9
Temperature (°F)	850	850
Reynolds' Number	7603	17740
Aspect Ratio	1.33	1.14

Table 10.3.1 -- Inlet Conditions

10.4 Perfectly-Stirred Reactor Model

The PSR model developed by Sandia National Laboratories [5] was utilized in this investigation. This program predicts steady-state temperature and species composition in a flow that is kinetically limited. As opposed to mixing limited flow, the PSR model assumes that the fuel and air are well mixed and that the rate of conversion from reactants to products is solely controlled by the chemical reaction rates. The reactor is characterized by its volume, residence time (or mass flow rate), heat loss (or temperature) and the inlet temperature and chemical composition of the flow. The use of this essentially non-dimensional (spatially) model allows for the use of a full chemical reaction mechanism, which provides more accurate predictions of temperature and species composition. The PSR program runs in conjunction with the CHEMKIN package [61] to handle the inclusion of the chemical mechanism.

The chemical reaction mechanism used in this study was the recently developed GRI mechanism (Version 1.2) [7] for methane. This version of the GRI Mechanism is exactly the same as the most recent version (Version 2.11), except that the nitrogen kinetics is not included. The inclusion of these reactions is not necessary since the minor species created through high temperature N_2 decomposition have little effect on heat release or ignition potential of the mixture, but would increase the difficulty in obtaining solution convergence.

Some modifications to the GRI mechanism were necessary in order to obtain a converged solution for the recirculation zones with fairly long residence times (i.e. $\tau > 10$ ms). These modifications included the removal of some minor and intermediate species (11 species total) from the reaction mechanism. These species were in such low concentrations in the final products that model convergence was inhibited.

As described above, the PSR program requires a number of inputs. Recirculation zone volume is obtained from the CFD results based on the velocity fields computed behind the step. A technique to determine the residence time of each recirculation zone was also developed and is described below. The recirculation zones were considered to be adiabatic in this analysis.

10.5 Residence Time and Volume Determination

Residence times for the individual recirculation zones were obtained utilizing the CFD model results. Similar to experimental studies which have measured recirculation zones behind bluff bodies [8,9], a passive scalar or marker is 'released' at the inlet to the flow being modeled and

allowed to arrive at some steady-state value throughout the flow. The passive scalar can be added to a converged CFD model, since the marker only tracks with the flow and has no interaction with the fluid. At some arbitrary time (e.g. $t = 0$), the flow of the marker is stopped and the concentration decay of the scalar is monitored within the recirculation zone. Assuming the recirculation zone is well mixed, the concentration of the marker will decay according to the following equation [8,9]:

$$\alpha = \alpha_e + C_o e^{-t/\tau} \quad \text{Equation 5}$$

where C_o is the initial concentration in excess of the input concentration α_e , and τ is the residence time or "filling" time for the reactor. The residence time (τ) is determined by curve-fitting the concentration decay curve found from the CFD results with an exponential of the form $A \exp(-Bt)$, with $\tau = 1/B$. The volume of the PSR is also determined from the CFD modeling by examining the recirculation zone. The volume for the recirculation zone is calculated by taking the flow volume contained inside the outermost region of flow reversal in the area of recirculating flow. Although this volume is somewhat dependent on the size of the mesh, the results were found to be insensitive to the selection of this volume.

10.6 Lean Blowout Criteria

The version of the Sandia PSR code used in this study did not provide a clear indication of when ignition of the mixture was not possible. Ideally, the code would indicate failure of ignition by showing little to no combustion products and little temperature rise in the outflow. However, the large number of stiff equations that must be solved in these large reaction mechanisms prevent such an elegant indication of the failure for ignition; generally, the equation solver would fail due to the very low concentrations of minor or intermediate species causing the solution to diverge. Hence, the development of suitable criteria for determining lean blowout from the PSR results is necessary.

An examination of experimental data from a number of studies [as described in Ref.1] led to the development of two possible criteria for establishing the blowout conditions; one based on temperature and one based on CO concentration. Experimental data show that as a flame approaches the blowout condition, the CO concentration starts to rise. This rise in CO occurs because the relatively low temperatures and short residence times, which accompany lean blowout, prevent complete oxidation of CO to CO₂ even though this conversion is favored by equilibrium. Additionally, the published results of lean blowout suggest that a minimum flame temperature is necessary to support combustion [see Ref. 1].

Based on examination of adiabatic flame temperatures at the lean flammability limit for several gaseous fuels and the results of several experimental studies, a minimum temperature of 1800K in the PSR model was adopted as a criterion for flameholding. This temperature was higher than used in the previous work [1] performed for CESI, but accounts for the higher preheat temperature. This temperature is considered to be conservative since, in the present application, even intermittent flameholding is undesirable. By using both the CO criterion and the minimum temperature, a range of potential flameholding equivalence ratios is created. The experimental data will be used to evaluate this range and criteria. Further reduction of this range will be possible after this evaluation.

10.7 Results and Discussion

Comparisons of the predicted flow fields (at various spanwise positions) for both the one-inch and two-inch sections are shown in Fig. F2, F3, F4, F5, and F6. These figures focus in on the recirculation zone behind the expansion. Velocity predictions for the entire section are included in Appendix F (Figs. F2 – F6). Accounting for the effects of scale, little difference on the flow field for either test section is seen as a function of distance from the wall, indicating that no large-scale spanwise flow movement is predicted. This is not unexpected, since k- ϵ models will not predict the vortical structure and subsequent boundary layer movement of these flows. However, experimental evidence has shown that for lower Reynolds flows (flows less than $Re = 6600$) significant spanwise flow can be induced [10].

Flow reattachment lengths downstream of the step were measured for both the 2-D and 3-D models. These lengths can be compared with values measured experimentally for similar flow geometries and provide an idea of the accuracy of the model. These lengths were determined by identifying the location of inflection of axial wall shear stress. Figures F7 and F8 show the distribution of wall shear stress for the 3-D models. Based on these distributions, non-dimensional reattachment lengths (distance from step/step height) are shown in Table 10.7.1. Results using the standard k- ϵ model using the Chen modification are included in the table. The Chen model was developed specifically for regions of high shear and improved these predictions considerably. Without the Chen modification, reattachment lengths were approximately 25% shorter than those shown in Table 10.7.1.

Section Size	Reattachment Length (X_r/H_s)	
	2-D	3-D
1-inch x 1-inch	6.56	6.88
2-inch x 2-inch	6.04	6.09

Table 10.7.1 -- Reattachment Length using the standard k- ϵ model with Chen modification

These lengths are very similar to those reported in the literature [10,11]. Armaly [10] report that for flows with Reynolds' numbers above ~ 6600 , the non-dimensional reattachment length is fairly constant at approximately 6.0. However, Chen and Jaw [11] state that the non-dimensional reattachment length is close to 7.0. Chen and Jaw [11] also state that most standard k- ϵ models under-predicting the reattachment length by at least 20 percent. The thickness of the boundary layer relative to the step height is an important concern for these models. For the 1-inch square section, the boundary layer was estimated to be approximately 15% of the step height, while for the 2-inch square section the boundary layer was a smaller percentage (10%) of the step height. Since the k- ϵ model does not handle flow in the boundary layer properly, much of the important information concerning the flow in the recirculation zone may be lost in this boundary layer thickness. This finding indicates that it is important to use the largest test section possible when experimentally obtaining comparison data in order to reduce the inherent errors of the models. Figures F9a, F9b, F10a, F10b, F11a, F11b, F12a, F12b, F13a, and F13b show the predicted spanwise (or in-plane) velocity gradients downstream from the expansion for the two test sections. Each downstream location has a vector and contour plot to aid in presenting the

velocity profiles. Overall, the 2-inch section predicts more significant spanwise flow behind the step than the smaller section. This may be due to the boundary layer thickness issue discussed previously. One important point to note is that experimental studies [12] have shown that if the expansion ratio (defined as the ratio of outlet height to inlet height) is equal or less than 1.5, turbulent flow is steady and separation is also symmetrical in a symmetric backward facing step. However, at expansion ratios greater than 1.5, the flow may become unsteady and unsymmetrical [11]. The expansion ratios chosen for this validation should avoid these problems.

10.7.1 Flameholding Analysis

Utilizing the analytical technique developed previously for CCSI, the flameholding potential of the predicted recirculation zones are analyzed. As described above, the flameholding analysis uses a comprehensive chemical kinetic mechanism and the flow characteristics of the recirculation zone. The CFD model results are used to obtain the parameters relating to the fluid mechanics. Table 10.7.1.1 presents the predicted recirculation time and recirculation zone volume for both the 2-D and 3-D models. The results of the flameholding analysis for both the 1-inch and 2-inch sections are shown in Fig. F14. The plot contains predictions of CO and temperature as a function of equivalence ratio using the residence time and volume of the recirculation zone shown in Table 10.7.1.1. As can be seen in the figure, very little difference in the flameholding potential is predicted for the various test section sizes. Using the flameholding criteria described above, the minimum equivalence ratio necessary for flameholding is approximately 0.485 to 0.53 for the 1-inch section and 0.49 to 0.53 for the 2-inch section. The fairly short recirculation times raise the minimum equivalence ratio necessary for flameholding.

	Test Section Model	Recirculation Zone Volume (in ³)	Recirculation Time (msec)
1-inch x 1-inch	2D	0.00957645	20.097
	3D	0.132091	20.984
2-inch x 2-inch	2D	0.0131413	20.93
	3D	0.2182	20.343

Table 10.7.1.1 -- Recirculation Zone Volume and Time

10.8 Summary and Conclusions

1-inch and 2-inch square sections containing a sudden expansion were modeled to determine the predicted differences in the flowfield and in the flameholding potential. Very little difference in the flowfield, other than the effect of scale, is predicted for these sections. Flameholding potential was also very similar for both test sections. From a modeling standpoint though, concerns about the ability of the k-ε model to adequately predict the recirculation zone and boundary layer velocities profiles reinforce the need for the experimental program to utilize the largest test section possible.

XI. Conclusions and Future Work

While significant progress was made towards developing an Axial Premixer for future CESI applications, further work will be needed in order to complete the design. The benefits of this study are listed as follows:

- The study gave a significant head-start towards the redesign and improvement of premixers for current and future Xonon® applications
- CESI gained a more thorough understanding of flame holding mechanisms for future iterations of Lobe premixers and other future CESI mixing hardware
- Further experience with cold flow rig test and data acquisition for axial premixers was acquired. In addition, the rig is readily available for future testing
- CESI gained detailed experience with the CFD simulation tool focused on Lobe Premixer analysis. In addition, detailed results from the parametric analysis will be very useful in current and future mixer development

Future work required for completion of the current axial premixer is given below:

- Conduct further analysis and cold rig testing in order to revised and optimize the axial premixer design.
- Complete fired engine hot-testing as detailed in Tasks 4.5 – 4.7.

References

References – Section 9

1. D.R. Ballal and A.H. Lefebvre (1979). Weak Extinction Limits of Turbulent Flowing Mixtures. *Journal of Engineering for Power*, Vol. 101, pp. 343-348.
2. A.B. Cambel and B.H. Jennings (1958). *Gas Dynamics*, McGraw Hill, New York.
3. P.R. Choudhury and A.B. Cambel (1962). Flame Stabilization by Wall Recesses, Flame Holding: Selected Engine Combustion Problems.
4. M. Gerstein (1958). *Proceedings, 3rd AGARD Colloquium on Combustion and Propulsion*, Pergamon Press, New York, pg. 307.
5. L.W. Huelmantel, R.W. Ziemer, and A.B. Cambel (1957). Stabilization of Premixed Propane-Air Flames in Recessed Ducts, *Jet Propulsion*, January.

References – Section 10

1. Roby, R. J. and Klassen, M. S., "Development of an Analytical Technique to Predict Flameholding in Gas Turbine Premixers", Report for CCSI, July 1998.
2. STAR*CD Version 3.05a User's Manuals, Computational Dynamics, London, England, 1998.
3. Norris, L. H. and Reynolds, W. C., "Turbulent Channel Flow with a Moving Wavy Boundary", Report No. FM-10, Dept. of Mechanical Engineering, Stanford University, 1975.
4. Chen, Y. S. and Kim, S. W., "Computation of Turbulent Flows Using an Extended k-epsilon Turbulence Closure Model, NASA CR-179204, 1987.
5. Glarborg, P., Kee, R. J., Grcar, J. F., and Miller, J.A., "PSR: A FORTRAN Program for Modeling Well-Stirred Reactors", Sandia National Laboratories Report SAND86-8209, 1991.
6. Kee, R. J., Miller, J. A., and Jefferson, T. H., "CHEMKIN: A General-Purpose Problem-Independent, Transportable, FORTRAN Chemical Kinetics Code Package, " Sandia National Laboratories Report SAND80-8003, 1980.
7. GRI Mechanism 1.2, http://www.diesel.fsc.psu.edu/~gri_mech
8. van der Lans, R. P., Glarborg, P., Dam-Johansen, K., and Larsen, P. S., Residence Time Distributions in a Cold, Confined Swirl Flow: Implications for Chemical Engineering Combustion Modeling, *Chem. Eng. Sci.* 52, pp. 2742-2756, 1997.
9. Roberds, D. W., McGregor, W. K., Hartsfield, B. W., Schulz, R. J., and Rhodes, R. P., Measurement of Residence Time, Air Entrainment Rate and Base Pressure in the Near Wake of a Cylindrical Body in Supersonic Flow, *AIAA J.* 27, pp. 1524-1529, 1989.
10. Armaly, B. F., Durst, F., Pereira, J. C. F., and Schonung, B., "Experimental and Theoretical investigation of backward-facing step flow", *J. Fluid Mech.* 127, pp. 473-496, 1983.
11. Chen, C-J and Jaw, S-Y, *Fundamentals of Turbulence Modeling*, Taylor & Francis, pp. 158-159, 1998.
12. Abott, D. E. and Kline, S.J., "Experimental investigation of subsonic flow over single and double backward facing steps", *J. Basic Engineering* 84, 317-325, 1992.